1. Extended Data

Figure #	Figure title One sentence only	Filename This should be the name the file is saved as when it is uploaded to our system. Please include the file extension. i.e.: *Smith_ED_Fig1.jpg*	Figure Legend If you are citing a reference for the first time in these legends, please include all new references in the main text Methods References section, and carry on the numbering from the main References section of the paper. If your paper does not have a Methods section, include all new references at the end of the main Reference list.
Extended Data Fig. 1	**High LHCGR expression in *GNA11* and *CTNNB1* double mutant co-transfected primary human adrenal cells.**	New_Extended_Data_Figure_1.tif	**a**, APA 351T cells transfected with *CTNNB1* (untagged plasmid) and *GNA11* (GFP-tagged plasmid) wild-type or Q209P (red boxed cell). LHCGR and CTNNB1 expression was visualized as in Figure 3f using the primary antibody rabbit anti-LHCGR #NLS1436 (1:200; Novus Biologicals, UK) and the primary antibody mouse anti-CTNNB1 #610154 (1:100; BD transduction Lab, USA), respectively. Scale bars, 50 µm. **b**, Immunofluorescence of LHCGR in APA 351T cells was quantified using corrected total cell fluorescence (CTCF). LHCGR expression was increased in cells expressing high CTNNB1 and GNA11 Q209P (the exact number, *n*, of cells quantified from two independent experiment are as indicated below the *x*-axis; the *P*-values indicated are according to Kolmogorov–Smirnov statistical test). High CTNNB1 was determined as CTCF >10,000. Data are presented as mean values +/- s.e.m.
Extended Data Fig. 2	***GNA11* somatic mutations were found in the adjacent adrenals to double-mutant APA of patient 6.**	New_Extended_Data Figure_2.tif	**a**, From six different regions (R1-5, at the edges of the adrenal cortex, R6 and APA, within the circled areas) in the formalin fixed paraffin embedded (FFPE) adjacent adrenal gland, genomic DNA samples of patient 6 were genotyped for *CTNNB1* and *GNA11* mutations. Immunohistochemistry of KCNJ5 and CYP11B2 were used for

			region selection. Scale bar, 10 mm and 50 µm as indicated. **b**, Sanger sequencing identified weak chromatogram peaks of *CTNNB1* G34R and *GNA11* Q209P somatic mutations in region 6 of the adjacent adrenal gland. **c**, Next generation sequencing confirmed the *CTNNB1* G34R and *GNA11* Q209P mutations in region 6 of the adjacent adrenal gland. **d**, qPCR of R1-6 and APA showed a 337-fold higher of *TMEM132E*, 38-fold higher of *CYP11B2*, 14-fold higher of *DKK1* and 10-fold higher of *LHCGR* expression in region 6 compared to region 5. Regions 1-5 have similar expression of the above genes. The APA had the highest expression of *CYP11B2, TMEM132E, DKK1, LHCGR* and lowest expression of *CYP11B1* and *LGR5* compared to regions 1-6.

2. Supplementary Information:

A. Flat Files

Item	**Present?**	**Filename** **This should be the name the file is saved as when it is uploaded to our system, and should include the file extension. The extension must be .pdf**	**A brief, numerical description of file contents.** **i.e.: *Supplementary Figures 1-4, Supplementary Discussion, and Supplementary Tables 1-4.***
Supplementary Information	Yes	New_Supplementary_Appendix.pdf	Supplementary Figures 1-6 and Supplementary Tables 1-9
Reporting Summary	Yes	NG-A55436R_Reporting_Summary.pdf	
Peer Review Information	Yes	*PRFile_Brown.pdf*	

3. Source Data

Parent Figure or Table	Filename This should be the name the file is saved as when it is uploaded to our system, and should include the file extension. i.e.: *Smith_SourceData_Fig1.xls,* or *Smith_ Unmodified_Gels_Fig1.pdf*	Data description i.e.: Unprocessed Western Blots and/or gels, Statistical Source Data, etc.
Source Data Fig. 2	New_Source_Data_for_Figure _2.xls	Statistical Source Data
Source Data Fig. 3	New_Source_Data_for_Figure _3.xls	Statistical Source Data

Somatic mutations of *GNA11* and *GNAQ* in *CTNNB1*-mutant aldosterone-producing adenomas presenting in puberty, pregnancy or menopause

Junhua Zhou[1,2,27], Elena A. B. Azizan[1,3,27*], Claudia P. Cabrera[2,4,27], Fabio Fernandes-Rosa[5,27], Sheerazed Boulkroun[5,27], Giulia Argentesi[1,2], Emily Cottrell[6], Laurence Amar[5,7], Xilin Wu[1,2], Sam O'Toole[1,2], Emily Goodchild[1,2], Alison Marker[8], Russell Senanayake[9], Sumedha Garg[1,2,9], Tobias Åkerström[10], Samuel Backman[10], Suzanne Jordan[11], Satyamaanasa Polubothu[12], Dan Berney[13], Anna Gluck[14], Kate E. Lines[14], Rajesh V. Thakker[14], Antoinette Tuthill[15], Caroline Joyce[16], Juan Pablo Kaski[17], Fiona Karet Frankl[18], Lou Metherell[6], Ada E. D. Teo[19], Mark Gurnell[9], Laila Parvanta[20], William M. Drake[21], Eva Wozniak[22], David Klinzing[23], Jyn Ling Kuan[23], Zenia Tiang[23,24], Celso E. Gomez Sanchez[25], Per Hellman[10], Roger Foo[23], Charles A. Mein[22], Veronica Kinsler[11], Peyman Björklund[10], Helen L. Storr[6,28], Maria-Christina Zennaro[5,26,28*], and Morris J. Brown[1,2,28*]

1. Endocrine Hypertension, Department of Clinical Pharmacology, William Harvey Research Institute, Queen Mary University of London, London, UK.
2. NIHR Barts Cardiovascular Biomedical Research Centre, Barts and The London School of Medicine and Dentistry, Queen Mary University of London, London, UK.

3. Department of Medicine, The National University of Malaysia (UKM) Medical Centre, Kuala Lumpur, Malaysia.
4. Centre for Translational Bioinformatics, William Harvey Research Institute, Queen Mary University of London, London, UK.
5. INSERM, U970, Paris Cardiovascular Research Center (PARCC), Paris, France.
6. Centre for Endocrinology, William Harvey Research Institute, Queen Mary University of London, London, UK.
7. Assistance Publique-Hôpitaux de Paris, Hôpital Européen Georges Pompidou, Unité Hypertension artérielle, Paris, France.
8. Department of Histopathology, Addenbrooke's Hospital, Cambridge, UK.
9. Metabolic Research Laboratories, Welcome Trust-MRC Institute of Metabolic Science, Cambridge Biomedical Campus, Cambridge, UK.
10. Department of Surgical Sciences, Uppsala University, Uppsala, Sweden.
11. Cellular Pathology Department, Royal London Hospital, London, UK.
12. Genetics and Genomic Medicine, University College London Great Ormond Street Institute of Child Health, London, UK.
13. Department of Molecular Oncology, Barts Cancer Institute, Queen Mary University of London, London, UK.
14. Academic Endocrine Unit, Radcliffe Department of Medicine, University of Oxford, Oxford, UK.
15. Department of Endocrinology and Diabetes, Cork University Hospital, Cork, Ireland.
16. Clinical Biochemistry, Cork University Hospital, Cork, Ireland.
17. Centre for Inherited Cardiovascular Diseases, Great Ormond Street Hospital and University College London Institute of Cardiovascular Science, London, UK.
18. Cambridge Institute for Medical Research, University of Cambridge, Cambridge, UK.
19. Dept of Medicine, Yong Loo Lin School of Medicine, National University of Singapore, Singapore.
20. Department of Surgery, St Bartholomew's Hospital, London, UK.

21. Department of Endocrinology, St Bartholomew's Hospital, London, UK.
22. Barts and London Genome Centre, School of Medicine and Dentistry, Blizard Institute, Queen Mary University of London, London, UK.
23. Cardiovascular Disease Translational Research Programme, Yong Loo Lin School of Medicine, National University of Singapore, Singapore.
24. Genome Institute of Singapore, Agency for Science, Technology and Research, Singapore.
25. G.V. (Sonny) Montgomery VA Medical Center and Department of Pharmacology and Toxicology, University of Mississippi Medical Center, Jackson, MS, USA.
26. Assistance Publique-Hôpitaux de Paris, Hôpital Européen Georges Pompidou, Service de Génétique, Paris, France.
27. These authors contributed equally.
28. These authors jointly supervised this work.
*email: elena.azizan@ukm.edu.my; maria-christina.zennaro@inserm.fr; morris.brown@qmul.ac.uk

Most aldosterone-producing adenomas (APA) have gain-of-function somatic mutations of ion-channels or transporters. However, their frequency in aldosterone-producing cell clusters of normal adrenals suggests a requirement for co-driver mutations in APAs. Here we identified gain-of-function mutations in both *CTNNB1* and *GNA11* by whole exome sequencing of 3/41 APAs. Further sequencing of known *CTNNB1*-mutant APAs led to a total of 16 of 27 (59%) with a somatic p.Gln209His, p.Gln209Pro or p.Gln209Leu mutation of *GNA11* or *GNAQ*. Solitary *GNA11* mutations were found in hyperplastic zona glomerulosa adjacent to double-mutant APAs. Nine of ten patients in our UK/Irish cohort presented in puberty, pregnancy, or menopause. Among multiple transcripts upregulated >10-fold in double-mutant APAs was *LHCGR*, the receptor for luteinizing or pregnancy hormone (human-chorionic-gonadotropin). Transfections of adrenocortical cells demonstrated additive effects of *GNA11* and *CTNNB1* mutations on aldosterone secretion and expression of genes upregulated in double-mutant APAs. In adrenal cortex, *GNA11/Q* mutations appear clinically silent without a co-driver mutation of *CTNNB1*.

Primary aldosteronism is a major cause of hypertension. This is potentially curable when due to an aldosterone-producing adenoma (APA) in one adrenal. Conversely, when primary aldosteronism is overlooked, it leads to resistant hypertension and high cardiovascular risk. The landmark report of somatic gain-of-function mutations in *KCNJ5* in 30-40% of APAs was followed by the discovery of further ion-channel or transporter mutations, mainly of *CACNA1D*, *ATP1A1* and *ATP2B3*, and of some clinical, pathological and biochemical differences between *KCNJ5*-mutant APAs and the others[1-4]. In particular, *KCNJ5*-mutant APAs are more common in women and have features resembling the cortisol-secreting cells of physiological zona fasciculata (ZF)[5-8]. Conversely, APAs with other ion-channel mutations are more common in men and resemble the physiological smaller aldosterone-producing cells of adrenal zona glomerulosa (ZG)[4,9]. Opinion has varied on whether the residual 20-30% of APAs without apparent mutation is due to sampling from parts of an APA that do not express

the aldosterone-synthesizing enzyme, CYP11B2, or to the existence of further somatic mutations yet to be discovered[8-10]. The genes whose mutation increases aldosterone production may differ from those responsible for tumor formation. Several of the former, particularly *CACNA1D*, are frequently mutated in the aldosterone-producing cell clusters (or nodules) of otherwise normal adrenals[11]. *KCNJ5* mutation was initially proposed to stimulate cell proliferation, as well as aldosterone production[1], but the increased calcium entry consequent on mutation stimulates apoptosis rather than proliferation[12]. Wnt pathway-activating mutations of *CTNNB1*, encoding β-catenin, are found in ~5% of APAs. β-catenin is a co-activator for a number of transcription factors, and mutations that prevent phosphorylation of exon-3 residues are regarded as oncogenic in adrenal and other tumors[8,10,13,14]. However, there are only rare reports of *CTNNB1* mutations co-existing with somatic mutations that activate aldosterone production[8,15], and in most APAs with *CTNNB1* mutations, these have been apparently solitary[13,16]. Whether *CTNNB1* mutations are able on their own to stimulate autonomous aldosterone production, or co-exist with other unidentified mutations, has not been resolved.

Three whole exome sequencing (WES) studies, which initially found *CACNA1D*, *ATP1A1*, and *ATP2B3* mutant APAs[2-4], also reported several other genes mutated in the tumor DNA. However, even re-interrogation of the three WES studies together did not identify additional potential pathogenic mutations that are present in more than one sample. We therefore undertook another WES study of tumor and germline DNA from a new cohort of 41 APA patients in order to determine whether there are further genes with recurrent somatic mutation, and whether these were associated with a specific clinical or biochemical phenotype.

Results

Identification of pathogenic somatic mutations in APAs. WES identified somatic mutations of the four ion-channel/transporter genes at known hotspots in 29 of the 41 APAs (**Supplementary Table 1**). Somatic mutations of *CACNA1D* were the most frequent (*n* = 11), followed by *KCNJ5* (*n* = 9), *ATP1A1* (*n* = 5) and *ATP2B3* (*n* = 4). Three APAs had a known mutation of *CTNNB1*. All three were noted to have a second mutation of the Q209 residue of *GNA11*, which encodes the G-protein G11. This, or the closely homologous Gq, mediates the aldosterone response to its principal physiological stimulus, angiotensin II (**Fig. 1a**), and the highly conserved p.Gln209 residue is essential for GTPase activation (**Fig. 1b**)[17,18]. These mutations cause constitutive G11/q activation.

Sanger sequencing and replication of *GNA11/Q* genotype. *UK/Ireland (discovery cohort).* We identified p.Gln209His or p.Gln209Pro mutations of *GNA11* in the APAs of four further patients in whom presentation in periods of high LH/HCG had prompted discovery of somatic mutations in exon 3 of *CTNNB1* (**Supplementary Fig. 1a**). One patient was indeed our index case of *CTNNB1* mutation, detected by our first WES, where the p.Gln209His mutation of *GNA11* was reported in the pair-wise comparison analysis[4]. Once we recognized the co-existence of mutations in *CTNNB1* and *GNA11*, and associated features reported herein, targeted sequencing identified somatic exon 3 mutations of *CTNNB1* and p.Gln209 mutations of either *GNA11* or closely homologous *GNAQ* in three further APAs (**Supplementary Fig. 1a**). Of the total cohort, one was a 12-year old boy presenting at puberty, and the other nine were women, with presentations in early pregnancy (*n* = 7) or menopause (*n* = 1). All ten were completely cured of hypertension post-adrenalectomy (**Table 1**).

French cohort. We examined 13 APAs from patients in France for mutation at p.Gln209 of either *GNA11* or *GNAQ*. These APAs had previously undergone targeted sequencing and been found to have somatic mutations at exon 3 of *CTNNB1.* Of these 13 APAs, three had mutations at p.Gln209 of *GNA11* and one at p.Gln209 of *GNAQ* (**Table 2** and **Supplementary Fig. 1b**). During the study, double-mutation was suspected in a fifth woman, aged 17, whose primary aldosteronism dated from

puberty; her APA was confirmed to have somatic mutation at p.Gly34 of *CTNNB1* and p.Gln209 of *GNAQ* (**Table 2** and **Supplementary Fig. 1b**). As controls, we genotyped a further nine APAs with known ion-channel/transporter gene mutations but found no mutation of *CTNNB1*. In none of these nine cases was a mutation found in *GNA11* or *GNAQ*.

Swedish cohort. We achieved further replication by re-analyzing RNA-seq FASTQ data from the APAs of a published cohort of 15 Swedish patients[19]. This included three APAs with somatic mutations of *CTNNB1.* The re-analysis found one of these to have a p.Gln209His mutation of *GNAQ* (**Table 2**). No mutation of *GNA11* or *GNAQ* was seen in the other 12 APAs that had one of the known ion-channel/transporter gene mutations[19].

In summary, 23/27 patients with *CTNNB1*-mutant APAs were women, and 16 of the 27 (59%) had a mutation at p.Gln209 of *GNA11* (*n* = 11) or *GNAQ* (*n* = 5). Among the latter, all were women except for the pubertal boy.

Functional analyses in human adrenocortical cells. H295R is an immortalized adrenocortical cell line heterozygous for the p.Ser45Pro mutation of *CTNNB1* but wild-type for *GNA11* (**Supplementary Fig. 2a**). Transfection of H295R cells by each of the *GNA11* mutations (**Supplementary Fig. 2b**) increased aldosterone secretion and *CYP11B2* expression (encoding aldosterone synthase) by 4.0-6.2-fold and 3.4-4.2-fold, respectively, compared to wild-type transfected cells (**Fig. 2a,b**). The stimulatory effect of angiotensin II 10 nM was retained in the mutant-transfected cells (**Supplementary Fig. 2c**). The stimulation of cortisol production by the mutations was less than of aldosterone (**Supplementary Fig. 2d,e**). In order to determine whether the Q209 mutations of *GNA11* stimulate aldosterone production, even in the absence of CTNNB1 activation, the transfections of H295R cells were repeated after either silencing of CTNNB1 using a Dharmacon SMARTpool siRNAs or 24-h treatment with the CTNNB1 inhibitor ICG-001[20,21]. Both interventions reduced the aldosterone production relative to vehicle-treated cells, as anticipated by published experiments (**Fig. 2c,d**)[22,23]. However,

neither silencing of CTNNB1 nor ICG-001 blunted the fold-increase in aldosterone secretion seen in mutant-transfected cells compared to wild-type (**Fig. 2c,d** and **Supplementary Fig. 2f**). As a further test of whether *GNA11* mutations require co-existing *CTNNB1* activation in order to increase aldosterone production, we used primary adrenocortical cells freshly dispersed from APAs with wild-type genotype for *CTNNB1* and *GNA11* (**Supplementary Table 2**). Cells were transfected with one each of the *CTNNB1* and *GNA11* mutants, or with both mutants together, and compared with cells transfected with vector or wild-type genes. Aldosterone secretion and CYP11B2 expression were increased by the individual mutations, but their combination caused substantially greater increases (**Fig. 2e** and **Supplementary Fig. 2g**). We also studied the p.Gln290His mutation of *GNAQ*. Its transfection into H295R cells increased aldosterone secretion by 1.93-fold (s.e.m. = 0.06) (**Fig. 2f**).

Biochemical phenotype of APAs with double mutations. *LHCGR expression.* We previously linked the presentation of the first three women at times of high circulating LH or HCG to high LHCGR expression by *CTNNB1*-mutant APAs[16]. To determine whether the association requires double-mutation of *CTNNB1* and *GNA11*, rather than *CTNNB1* mutation alone, we performed qPCR of *LHCGR* in all *CTNNB1*-mutant APAs from the three cohorts. Fold-changes >10 (compared to available controls for each cohort) were seen in 15/16 double-mutant APAs (**Fig. 3a-c**). The exception, patient 10, was the sole patient with a p.Gln209Leu mutation. Of possible note, her adrenalectomy coincided with menstruation, when LHCGR expression, at least in ovarian follicles, is suppressed to <10% of maximum[24]. Conversely, 7/9 single-mutant APAs had low or undetectable *LHCGR* mRNA (P = 0.0001, Fisher exact test).

APAs from the ten UK/Irish patients were positive for LHCGR on immunohistochemistry (IHC) (**Fig. 3d** and **Supplementary Fig. 3a**). Expression within APAs was variable, particularly in APAs with variable expression of CYP11B2. In the APA from patient 10, which had low mRNA expression for *LHCGR*, the protein was concentrated in a visually distinct segment; this allowed demonstration that

192 variation in IHC signal corresponded to fold-change on qPCR (**Supplementary Fig. 3a**). Adrenal
193 medulla was also unexpectedly positive, confirmed by analyses of laser-capture microdissected RNA
194 (**Supplementary Fig. 3b**). Since LHCGR in steroidogenic cells is coupled to both GαS and GαQ/11, the
195 consequences of activation will depend not only on LH/HCG levels, but also on downstream
196 signalling, and paracrine stimulation by other cell types with physiological expression of LHCGR[25].
197 There was also striking heterogeneity in subcellular sites of expression (**Supplementary Fig. 3c**).
198 Membranous and vesicular expression were most common in double-mutant APAs, but cytosolic in
199 adjacent ZG (**Supplementary Fig. 3d**).

200 There is no expression of LHCGR in H295R cells, indicating that LH/HCG stimulation is not
201 essential in these cells to the induction of autonomous aldosterone production by *GNA11/Q*
202 mutation (**Fig. 2a-b,f** and **Supplementary Fig. 3e**). The steroidome of H295R cells suggests a cell of
203 origin in zona reticularis, far downstream of the primordial adrenogenital cells that are the common
204 precursor of gonads and adrenal cortex[26]. We therefore turned again to primary adrenocortical cells,
205 comparing LHCGR expression in cells transfected with mutant GNA11 and CTNNB1, alone or
206 together. qPCR showed greater expression of *LHCGR* in cells transfected with mutations of both
207 genes, than with single-mutations or vector (**Fig. 3e**). The low transfection of primary cells also
208 enabled comparisons of individual cells, by immunofluorescence, both within and between each
209 well. The red immunofluorescence for LHCGR was qualitatively intense, and frequently
210 membranous, in cells positive for both mutations, but was scarce in GFP-negative cells lacking
211 *GNA11* p.Gln209 mutation (**Fig. 3f** and **Supplementary Fig. 3e-i**). Quantitative analysis confirmed a
212 higher LHCGR intensity in cells with *GNA11*-mutant transfection (**Fig. 3g**). However some *GNA11*-
213 mutant cells were LHCGR positive even without *CTNNB1* transfection. Post-hoc analysis showed that
214 LHCGR (red) intensity was qualitatively and quantitatively associated with immunofluorescence
215 (magenta) for CTNNB1 (**Supplementary Fig. 3j**), consistent with adrenocortical Wnt activation in
216 primary aldosteronism[27,28]. When both plasmids were transfected into primary adrenocortical cells,
217 and these were compared by intensity of green (GNA11) and magenta (CTNNB1), the red (LHCGR)

intensity was 31-144 fold higher in cells with GNA11-p.Gln209Pro transfection and high CTNNB1 intensity than in other cells (**Extended Data Fig. 1**).

Expression of top differentiated genes. LHCGR was the most upregulated gene (compared to other APAs in the same microarray)[16] in the APA of patient 4, but a weaker pregnancy association in the replication cohorts (**Tables 1** and **2**) prompted us to ask whether there are other genes consistently upregulated in the double-mutant APAs. We re-examined our previous public-domain expression data (microarray or RNA-seq) performed in three of the double-mutant APAs before their genotype was known: the index case from 2013 (patient 4)[4,29,30], the APA from a menopausal woman (patient 6)[5], and the newly diagnosed Swedish double-mutant APA (S1)[19]. Unsupervised hierarchical clustering analysis of the most variably expressed genes in the three studies showed clustering of the three double-mutant APAs, and a high proportion of genes were many-fold upregulated compared to other APAs (**Fig. 4a**). *LHCGR* is among several 'hallmark' genes with uniquely high expression in the three double-mutant APAs, including the neuronal cell adhesion molecule *TMEM132E* and the Wnt inhibitor *DKK1* (**Fig. 4b**). Further genes are also upregulated in other ZG-like (compared to *KCNJ5*-mutant) APAs, or in one or both solitary *CTNNB1*-mutant APAs. A small number of genes are downregulated in the double-mutant APAs, including *CYP11B1* (**Fig. 4b**). This gene encodes the final enzyme in cortisol synthesis (11 β-hydroxylase). Enrichment analysis using DAVID (Database for Annotation, Visualization and Integrated Discovery v6.8) showed significant enrichment of features or terms concerned with cell-junction/cell adhesion or synapse (**Supplementary Table 3**).

qPCR confirmed large (10's to 1000's-fold) higher expression of several of the hallmark transcripts in 4-5 double-mutants (from whom RNA of fresh-frozen tissue remained) than in nine APAs without mutations of either gene (**Fig. 4c,d**) or (for *TMEM132E*) than in seven APAs with solitary mutation of *CTNNB1* (**Fig. 4e**). However, in H295R cells that were transfected with mutant *GNA11* and that have germline S45P mutation of *CTNNB1*, *TMEM132E* was the only one of the six

243 tested genes to be significantly and substantially upregulated (**Fig. 4f**). *TMEM132E* and *LHCGR* were
244 the top genes that differed most robustly between double-mutant and other APAs, including those
245 with solitary mutations of *CTNNB1* (**Fig. 4e** and **Supplementary Fig. 4**). LHCGR itself remained
246 undetectable after transfection of mutant *GNA11*.

247 In a previous IHC analysis of eight *CTNNB1*-mutant APAs, we reported four with low
248 CYP11B2 (H-score < 30) and high CYP11B1 expression (H-score > 200) versus three with high
249 CYP11B2 (H-score > 200) and low CYP11B1 expression (H-score < 1)[13]. No genotyping was available
250 from these patients, but IHC in two of the current Swedish cohort showed similar contrast between
251 the single- and double-mutant APAs (**Supplementary Fig. 5a**), supported by qPCR and aldosterone
252 measurements (**Supplementary Fig. 5b**). These findings, and the low *CYP11B1* expression highlighted
253 in the heatmap of the three double-mutant APAs (**Fig. 4b**), prompted us to analyze *CYP11B1* and
254 *CYP11B2* expression in double-mutant APAs compared to APAs with single mutations of *CTNNB1* or
255 other genotypes. qPCR confirmed a low *CYP11B1*:*CYP11B2* ratio, and an overall low expression of
256 *CYP11B1*, in ten double-mutant APAs with available RNA (**Fig. 5a**). IHC of all the UK/Irish double-
257 mutant APAs showed absent CYP11B1 but strong staining of CYP11B2 (**Fig. 5b**).

258

259 **Phenotype and genotype of adjacent adrenals.** The IHC also showed consistent hyperplasia of
260 adjacent ZG, with absence of both CYP11B1 and CYP11B2 staining, but weak/moderate staining for
261 LHCGR (**Supplementary Fig. 5c**). There were few aldosterone-producing cell clusters (APCCs), and a
262 possible atrophy of zona fasciculata (ZF). The ZG expansion resembles that in mice with transgenic
263 activation of adrenal Gq or CTNNB1[31,32]. A similar picture is also seen in a minority of patients with
264 mosaicism of *GNAS* at the residues analogous to the p.Gln209 or p.Arg183 residues of *GNA11/Q*
265 (McCune-Albright syndrome)[33-35]. We therefore wondered whether loci of *GNA11* mutation may be
266 present in the adrenal cortex adjacent to APAs with *GNA11* mutations at p.Gln209.

Multiple punch biopsies were taken for genomic DNA (± cDNA sequencing and qPCR) from six regions of fresh-frozen adrenal available from patient 7 (**Fig. 6a-c**). Genomic DNA from three regions had the same double-mutation genotype as the original tumor (**Supplementary Fig. 6a**); in one case, the associated cDNA had low expression of *CYP11B2* and *LHCGR* (**Fig. 6b**). Samples from the other three regions were *CTNNB1* wild-type, but one (DNA1) had the same p.Gln209His mutation of *GNA11* as the APA, homozygous in R1 genomic DNA and heterozygous in R1 cDNA (**Supplementary Fig. 6a** and **Fig. 6c**). The latter had undetectable levels of *CYP11B2*, *LHCGR* (**Fig. 6b**) and other hallmark differentially expressed genes (DEG) high in double-mutant APAs (**Supplementary Fig. 6a**), confirming its separation from the APA. In patient 6, a focal area of peri-medullary ZG cells was weakly positive for CYP11B2 (**Extended Data Fig. 2a**) and for mutations of *GNA11* and *CTNNB1* (**Extended Data Fig. 2b,c**). qPCR from this double-mutant region showed intermediate expression of several DEG genes (**Extended Data Fig. 2d**). For more precise analysis and location, we undertook laser capture microdissection (LCM) of a formalin-fixed paraffin embedded adrenal section from patient 1, in which ZG was intact in the adjacent adrenal gland (**Fig. 6d,e**). Two of eight sites (ZG1 and ZG6) at distinct ends of the adrenal limbs were, respectively, heterozygous or homozygous for the same p.Gln209Pro mutation in *GNA11* as the APA, but did not have the APA's mutation of *CTNNB1* (**Fig. 6f** and **Supplementary Fig. 6b**). The findings of APA mutations in adjacent adrenal were replicated in each case by up to three quantitative techniques (ddPCR for *GNA11* and *GNAQ*, targeted NGS for both tumor genes, and WES) (**Supplementary Table 4a-d**). There was high concordance between ddPCR, NGS and Sanger sequencing when analyzed in the same sample, e.g. in patient 6 (**Extended Data Fig. 2b,c** and **Supplementary Table 4a**). Where fresh samples were re-taken, concordance with Sanger sequencing was lower, e.g. patient 1 (**Fig. 6d-f** and **Supplementary Table 4b**) and patient 7 (**Supplementary Table 4a,b**), and NGS detected both tumor genes in some samples. Minor allele frequencies (MAF) > 3% were not seen for other bases in the targeted region or at the same base in other adrenals. No mutations were found in four adrenals adjacent to APAs

with *KCNJ5* or *CACNA1D* mutations (**Supplementary Table 4d**), nor in a limited number of scrapings adjacent to the double-mutant APAs from patients 2, 8, and 9 (**Supplementary Table 4b,c**).

In McCune-Albright syndrome, *GNAS* mutation can be difficult to detect, and appear homozygous, heterozygous or absent at adjacent sites[36,37]. Finding an APA's mutation at disparate sites of adjacent ZG could point to an origin during adrenogenesis, but strictly defined mosaicism is hard to prove within single tissues.

Discussion

We report the discovery of gain-of-function mutations of the G-protein gene *GNA11,* or its close homolog *GNAQ*, in multiple APAs. To date, the mutation is always residue p.Gln209 and associated with a gain-of-function mutation of *CTNNB1.* Mutation of p.Gln209, or homologous p.Gln in GNAS or GNA12-14, impair hydrogen bonds between G-protein α and β subunits[17,18]. In ZG, Gq/11 mediate the aldosterone response to angiotensin II via stimulation of intracellular Ca^{2+} release by inositol trisphosphate (IP3)[38]. Somatic mutations of the Gln209 or Arg183 codons of *GNA11* or *GNAQ* have been reported in the majority of uveal melanomas and in several congenital skin or vascular lesions, including blue nevi and Sturge-Weber syndrome[39-41]. In some congenital lesions, the mutation of *GNA11/Q* is mosaic, being found in several disparate sites[42].

The role of Wnt signalling in adrenal development and APA formation is well established[28,43,44]. Usually the Wnt activation in APAs is present without mutation of *CTNNB1*, but gain-of-function somatic mutations of exon 3 of *CTNNB1* are found in ~5% of APAs, as well as other adrenal tumors[10,13,14,27,45,46]. 20-30% of malignant adrenocarcinomas of the adrenal (ACC) have the same mutations of *CTNNB1* as occur in APAs[27], but mutations of *GNA11/Q* are absent from ACCs, and their common co-driver mutations are in different genes (e.g. *TP53*, *MED12*)[47]. In many malignancies, co-drivers are the exception, often following chemotherapy[48,49].

So why do these two well known oncogenic mutations cluster in APAs, but seemingly no other tumor? Occasional APAs have been reported with dual mutation of *CTNNB1* and *CACNA1D*[50]. However, unlike *GNA11/Q*, *CACNA1D* appears to be the sole driver in most APAs where it is mutated, or to co-exist with such a variety of mutations that no other gene was recurrently co-mutated in our 11 *CACNA1D*-mutant APAs. The greater prevalence of *CTNNB1* than *GNA11/Q* mutations, and the ZG hyperplasia of mice with *CTNNB1* mutations, might suggest that *GNA11/Q* mutations arise in a subset of *CTNNB1*-mutant APAs[51]. In possible support, Wnt activation by germline mutation of *APC* predisposes, rarely, to somatic mutation of *KCNJ5*[52]. In possible opposition is the high CYP11B1 expression of solitary *CTNNB1*-mutant APAs, but exceptionally low expression in the double-mutants, suggesting different sites of origin within the adrenal cortex.

The clue to whether one mutation generally precedes the other may come from growing evidence that increased transcription drives mutation[53], and from examples where Gq/11 lie upstream of CTNNB1 activation. As proof-of-concept, mutation of upstream *MAPK* in the melanogenesis pathway leads via second-hit mutation of *CTNNB1* to penetrating nevi[54]. A recent study of p.Gln209 mutations of *GNAQ* in uveal melanoma suggested that these cause hyperplasia, 'being insufficient for neoplastic transformation', and highlighted clustering of driver mutations within KEGG pathways to explain recurrent second hits[55]. Coincidentally, GNA11/Q and CTNNB1 feature together in just one KEGG pathway, melanogenesis. Adrenal MC1R expression, and presence of melanin in occasional pigmented adrenal nodules, seems unlikely to be directly relevant to our double-mutant APAs[56,57], but the connection between *GNAQ* and *CTNNB1* in melanogenesis is the Wnt receptor FZD6, which is the most upregulated Frizzled in ZG[29]. An additional potential link between Gq/11 and *CTNNB1* activation is through RSPO3[58]. The RSPO3-LGR5 pathway is active in ZG, maybe controlling cell proliferation and migration as in intestinal crypts[29,59-61]. In summary, *GNA11/Q* mutations may arise early and create conditions in which a second hit in *CTNNB1* leads to APA formation. Proven examples of *GNA11/Q* mosaicism, and the disconnected, discrete areas of *GNA11* mutation in adjacent hyperplastic ZG, are consistent with this view[42]. *CTNNB1* mosaicism has

342 occasionally been suggested, and much further work is required to determine whether mosaicism
343 for either or both genes might be the antecedent to double-mutant APAs[62,63]. A case of *KCNJ5*
344 mosaicism was recently reported[64].

345 In the replication cohorts from France and Sweden, single-mutant outnumbered double-
346 mutant APAs by 2:1, whereas no single-mutant APAs were found among UK patients. The latter
347 came from a variety of endocrine, renal and hypertension clinics, with no apparent referral bias.
348 Ethnic variation in somatic mutation of several genes is recognized in APAs, with *KCNJ5* mutations
349 being more common in cohorts of East Asian ancestry than those of European ancestry, and less
350 frequent than *CACNA1D* in patients of African ancestry, in whom no *CTNNB1* mutations are yet
351 reported[50,65]. Ancestral variation within Europe may seem less likely than between continents.
352 Although melanogenesis is probably irrelevant to adrenal p.Gln209 mutation, *MC1R* genotype and
353 phenotype (red hair) illustrate intra-continental heterogeneity[66].

354 Our findings suggest that onset of hypertension in the first trimester – the period of peak
355 HCG secretion – should prompt consideration of primary aldosteronism. Most pregnancy-associated
356 hypertension arises in later trimesters. The index case of our original report was successfully
357 managed on amiloride through pregnancy, whereas undiagnosed primary aldosteronism is high-risk
358 for mother and fetus[16,67]. We previously linked the seemingly explosive presentation of *CTNNB1*-
359 mutant APAs in early pregnancy to their induction of LHCGR expression. We have not ourselves
360 confirmed LH responsiveness of cells transfected with mutant CTNNB1 and GNA11, but LH can
361 induce the CYP11B2 promoter by 25-fold in adrenocortical cells transfected with LHCGR
362 expression[16,68]. LH stimulates modest increases in aldosterone secretion in some patients with
363 primary aldosteronism, and LHCGR is indeed commonly expressed in APAs and adjacent adrenal –
364 though at a much lower level than in our *CTNNB1*-mutant APAs presenting in pregnancy[16,69,70].
365 Subsequently, it became apparent that *CTNNB1* mutation was usually insufficient to cause the
366 phenotype of LH/HCG-dependent primary aldosteronism[69,71,72]. Our finding of a second driver

mutation explains much of the discrepant experience. Although the APA transcriptomes, and transfections of primary cells, show some overlap between phenotypes of single- and double-mutation, we infer that a double-hit within related pathways is more likely than a single-hit to cause large increases in expression of *LHCGR* and of other genes that may influence clinical presentation.

References

1. Choi, M. et al. K+ channel mutations in adrenal aldosterone-producing adenomas and hereditary hypertension. *Science* **331**, 768-772 (2011).
2. Beuschlein, F. et al. Somatic mutations in *ATP1A1* and *ATP2B3* lead to aldosterone-producing adenomas and secondary hypertension. *Nat. Genet.* **45**, 440-444 (2013).
3. Scholl, U. I. et al. Somatic and germline *CACNA1D* calcium channel mutations in aldosterone-producing adenomas and primary aldosteronism. *Nat. Genet.* **45**, 1050-1054 (2013).
4. Azizan, E. A. et al. Somatic mutations in *ATP1A1* and *CACNA1D* underlie a common subtype of adrenal hypertension. *Nat. Genet.* **45**, 1055-1060 (2013).
5. Azizan, E. A. et al. Microarray, qPCR and *KCNJ5* sequencing of aldosterone-producing adenomas reveal differences in genotype and phenotype between zona glomerulosa- and zona fasciculata-like tumors. *J. Clin. Endocrinol. Metab.* **97**, E819-E829 (2012).
6. Monticone, S. et al. Immunohistochemical, genetic and clinical characterization of sporadic aldosterone-producing adenomas. *Mol. Cell. Endocrinol.* **411**, 146-154 (2015).
7. Akerstrom, T. et al. Novel somatic mutations and distinct molecular signature in aldosterone-producing adenomas. *Endocr. Relat. Cancer* **22**, 735-744 (2015).
8. De Sousa, K. et al. Genetic, cellular, and molecular heterogeneity in adrenals with aldosterone-producing adenoma. *Hypertension* **75**, 1034-1044 (2020).
9. Nanba, K. et al. Targeted molecular characterization of aldosterone-producing adenomas in White Americans. *J. Clin. Endocrinol. Metab.* **103**, 3869-3876 (2018).
10. Wu, V. C. et al. The prevalence of *CTNNB1* mutations in primary aldosteronism and consequences for clinical outcomes. *Sci. Rep.* **7**, 39121 (2017).
11. Nishimoto, K. et al. Aldosterone-stimulating somatic gene mutations are common in normal adrenal glands. *Proc. Natl. Acad. Sci. USA* **112**, E4591-E4599 (2015).
12. Williams, T.A. et al. Visinin-like 1 is upregulated in aldosterone-producing adenomas with *KCNJ5* mutations and protects from calcium-induced apoptosis. *Hypertension* **59**, 833-839 (2012).
13. Akerstrom, T. et al. Activating mutations in *CTNNB1* in aldosterone producing adenomas. *Sci. Rep.* **6**, 19546 (2016).
14. Tadjine, M., Lampron, A., Ouadi, L. & Bourdeau, I. Frequent mutations of beta-catenin gene in sporadic secreting adrenocortical adenomas. *Clin. Endocrinol. (Oxf)* **68**, 264-270 (2008).
15. Omata, K. et al. Cellular and genetic causes of idiopathic hyperaldosteronism. *Hypertension* **72**, 874-880 (2018).
16. Teo, A. E. et al. Pregnancy, primary aldosteronism, and adrenal *CTNNB1* mutations. *N. Engl. J. Med.* **373**, 1429-1436 (2015).
17. Kalinec, G., Nazarali, A. J., Hermouet, S., Xu, N. & Gutkind, J. S. Mutated alpha subunit of the Gq protein induces malignant transformation in NIH 3T3 cells. *Mol. Cell. Biol.* **12**, 4687-4693 (1992).
18. Gutowski, S. et al. Antibodies to the alpha q subfamily of guanine nucleotide-binding regulatory protein alpha subunits attenuate activation of phosphatidylinositol 4,5-bisphosphate hydrolysis by hormones. *J. Biol. Chem.* **266**, 20519-20524 (1991).
19. Backman, S. et al. RNA sequencing provides novel insights into the transcriptome of aldosterone producing adenomas. *Sci. Rep.* **9**, 6269 (2019).
20. Wiese, M. et al. The beta-catenin/CBP-antagonist ICG-001 inhibits pediatric glioma tumorigenicity in a Wnt-independent manner. *Oncotarget* **8**, 27300-27313 (2017).
21. Zhou, L. et al. Multiple genes of the renin-angiotensin system are novel targets of Wnt/beta-catenin signaling. *J. Am. Soc. Nephrol.* **26**, 107-120 (2015).
22. Doghman, M., Cazareth, J. & Lalli, E. The T cell factor/beta-catenin antagonist PKF115-584 inhibits proliferation of adrenocortical carcinoma cells. *J. Clin. Endocrinol. Metab.* **93**, 3222-3225 (2008).

23. Zhou, T. et al. CTNNB1 knockdown inhibits cell proliferation and aldosterone secretion through inhibiting Wnt/beta-catenin signaling in H295R cells. *Technol. Cancer Res. Treat.* **19**, 1533033820979685 (2020).
24. Jeppesen, J. V. et al. LH-receptor gene expression in human granulosa and cumulus cells from antral and preovulatory follicles. *J. Clin. Endocrinol. Metab.* **97**, E1524-E1531 (2012).
25. Breen, S. M. et al. Ovulation involves the luteinizing hormone-dependent activation of G(q/11) in granulosa cells. *Mol. Endocrinol.* **27**, 1483-1491 (2013).
26. Gazdar, A. F. et al. Establishment and characterization of a human adrenocortical carcinoma cell line that expresses multiple pathways of steroid biosynthesis. *Cancer Res.* **50**, 5488-5496 (1990).
27. Tissier, F. et al. Mutations of beta-catenin in adrenocortical tumors: activation of the Wnt signaling pathway is a frequent event in both benign and malignant adrenocortical tumors. *Cancer Res.* **65**, 7622-7627 (2005).
28. Boulkroun, S. et al. Aldosterone-producing adenoma formation in the adrenal cortex involves expression of stem/progenitor cell markers. *Endocrinology* **152**, 4753-4763 (2011).
29. Shaikh, L. H. et al. LGR5 activates noncanonical Wnt signaling and inhibits aldosterone production in the human adrenal. *J. Clin. Endocrinol. Metab.* **100**, E836-E844 (2015).
30. Zhou, J. et al. Transcriptome pathway analysis of pathological and physiological aldosterone-producing human tissues. *Hypertension* **68**, 1424-1431 (2016).
31. Taylor, M. J. et al. Chemogenetic activation of adrenocortical Gq signaling causes hyperaldosteronism and disrupts functional zonation. *J. Clin. Invest.* **130**, 83-93 (2020).
32. Leng, S. et al. beta-Catenin and FGFR2 regulate postnatal rosette-based adrenocortical morphogenesis. *Nat. Commun.* **11**, 1680 (2020).
33. Schwindinger, W. F., Francomano, C. A. & Levine, M. A. Identification of a mutation in the gene encoding the alpha subunit of the stimulatory G protein of adenylyl cyclase in McCune-Albright syndrome. *Proc. Natl. Acad. Sci. USA* **89**, 5152-5156 (1992).
34. Weinstein, L. S. et al. Activating mutations of the stimulatory G protein in the McCune-Albright syndrome. *N. Engl. J. Med.* **325**, 1688-1695 (1991).
35. Idowu, B. D. et al. A sensitive mutation-specific screening technique for *GNAS1* mutations in cases of fibrous dysplasia: the first report of a codon 227 mutation in bone. *Histopathology* **50**, 691-704 (2007).
36. Vasilev, V. et al. McCune-Albright syndrome: a detailed pathological and genetic analysis of disease effects in an adult patient. *J. Clin. Endocrinol. Metab.* **99**, E2029-E2038 (2014).
37. Rey, R. A. et al. Unexpected mosaicism of R201H-GNAS1 mutant-bearing cells in the testes underlie macro-orchidism without sexual precocity in McCune-Albright syndrome. *Hum. Mol. Genet.* **15**, 3538-3543 (2006).
38. Wu, D. Q., Lee, C. H., Rhee, S. G. & Simon, M. I. Activation of phospholipase C by the alpha subunits of the Gq and G11 proteins in transfected Cos-7 cells. *J. Biol. Chem.* **267**, 1811-1817 (1992).
39. Ayturk, U. M. et al. Somatic activating mutations in *GNAQ* and *GNA11* are associated with congenital hemangioma. *Am. J. Hum. Genet.* **98**, 789-795 (2016).
40. Van Raamsdonk, C. D. et al. Mutations in *GNA11* in uveal melanoma. *N. Engl. J. Med.* **363**, 2191-2199 (2010).
41. Shirley, M. D. et al. Sturge-Weber syndrome and port-wine stains caused by somatic mutation in *GNAQ*. *N. Engl. J. Med.* **368**, 1971-1979 (2013).
42. Thomas, A. C. et al. Mosaic activating mutations in *GNA11* and *GNAQ* are associated with phakomatosis pigmentovascularis and extensive dermal melanocytosis. *J. Invest. Dermatol.* **136**, 770-778 (2016).
43. Simon, D. P. & Hammer, G. D. Adrenocortical stem and progenitor cells: implications for adrenocortical carcinoma. *Mol. Cell. Endocrinol.* **351**, 2-11 (2012).

44. Berthon, A. et al. WNT/beta-catenin signalling is activated in aldosterone-producing adenomas and controls aldosterone production. *Hum. Mol. Genet.* **23**, 889-905 (2014).
45. Lerario, A. M., Moraitis, A. & Hammer, G. D. Genetics and epigenetics of adrenocortical tumors. *Mol. Cell. Endocrinol.* **386**, 67-84 (2014).
46. Wang, J. J., Peng, K. Y., Wu, V. C., Tseng, F. Y. & Wu, K. D. *CTNNB1* mutation in aldosterone producing adenoma. *Endocrinol. Metab. (Seoul)* **32**, 332-338 (2017).
47. Assie, G. et al. Integrated genomic characterization of adrenocortical carcinoma. *Nat. Genet.* **46**, 607-612 (2014).
48. Jakobsen, J. N., Santoni-Rugiu, E., Grauslund, M., Melchior, L. & Sorensen, J. B. Concomitant driver mutations in advanced *EGFR*-mutated non-small-cell lung cancer and their impact on erlotinib treatment. *Oncotarget* **9**, 26195-26208 (2018).
49. Gainor, J. F. et al. *ALK* rearrangements are mutually exclusive with mutations in *EGFR* or *KRAS*: an analysis of 1,683 patients with non-small cell lung cancer. *Clin. Cancer Res.* **19**, 4273-4281 (2013).
50. Nanba, K. et al. Genetic characteristics of aldosterone-producing adenomas in Blacks. *Hypertension* **73**, 885-892 (2019).
51. Pignatti, E. et al. Beta-catenin causes adrenal hyperplasia by blocking zonal transdifferentiation. *Cell Rep.* **31**, 107524 (2020).
52. Vouillarmet, J. et al. Aldosterone-producing adenoma with a somatic *KCNJ5* mutation revealing APC-dependent familial adenomatous polyposis. *J. Clin. Endocrinol. Metab.* **101**, 3874-3878 (2016).
53. Polak, P. et al. Cell-of-origin chromatin organization shapes the mutational landscape of cancer. *Nature* **518**, 360-364 (2015).
54. Yeh, I. et al. Combined activation of MAP kinase pathway and beta-catenin signaling cause deep penetrating nevi. *Nat. Commun.* **8**, 644 (2017).
55. Piaggio, F. et al. Secondary somatic mutations in G-protein-related pathways and mutation signatures in uveal melanoma. *Cancers (Basel)* **11**, 1688 (2019).
56. Chen, X. et al. The melanoma-linked "redhead" MC1R influences dopaminergic neuron survival. *Ann. Neurol.* **81**, 395-406 (2017).
57. Cavlan, D., Storr, H. L., Berney, D., Evagora, C. & King, P .J. Adrenal pigmentation in PPNAD is a result of melanin deposition and associated with upregulation of the melanocortin 1 receptor. *Endocrine Abstracts* **38**, 154 (2015).
58. Binder, J. X. et al. COMPARTMENTS: unification and visualization of protein subcellular localization evidence. *Database (Oxford)* **2014**, bau012 (2014).
59. de Lau, W. et al. Lgr5 homologues associate with Wnt receptors and mediate R-spondin signalling. *Nature* **476**, 293-297 (2011).
60. Vidal, V. et al. The adrenal capsule is a signaling center controlling cell renewal and zonation through Rspo3. *Genes Dev.* **30**, 1389-1394 (2016).
61. Yi, H., Wang, Y., Kavallaris, M. & Wang, J. Y. Lgr4-mediated potentiation of Wnt/β-catenin signaling promotes MLL leukemogenesis via an Rspo3/Wnt3a-Gnaq pathway in leukemic stem cells. *Blood* **122**, 887 (2013).
62. Carter, J. M. et al. *CTNNB1* mutations and estrogen receptor expression in neuromuscular choristoma and its associated fibromatosis. *Am. J. Surg. Pathol.* **40**, 1368-1374 (2016).
63. Crago, A. M. et al. Near universal detection of alterations in CTNNB1 and Wnt pathway regulators in desmoid-type fibromatosis by whole-exome sequencing and genomic analysis. *Genes Chromosomes Cancer* **54**, 606-615 (2015).
64. Maria, A. G. et al. Mosaicism for *KCNJ5* causing early-onset primary aldosteronism due to bilateral adrenocortical hyperplasia. *Am. J. Hypertens.* **33**, 124-130 (2020).
65. Zhang, E. D. et al. Mutation spectrum in *GNAQ* and *GNA11* in Chinese uveal melanoma. *Precis. Clin. Med.* **2**, 213-220 (2019).

66. Gerstenblith, M. R., Goldstein, A. M., Fargnoli, M. C., Peris, K. & Landi, M. T. Comprehensive evaluation of allele frequency differences of *MC1R* variants across populations. *Hum. Mutat.* **28**, 495-505 (2007).
67. Eguchi, K. et al. An adverse pregnancy-associated outcome due to overlooked primary aldosteronism. *Intern. Med.* **53**, 2499-2504 (2014).
68. Saner-Amigh, K. et al. Elevated expression of luteinizing hormone receptor in aldosterone-producing adenomas. *J. Clin. Endocrinol. Metab.* **91**, 1136-1142 (2006).
69. Gagnon, N. et al. Genetic characterization of GnRH/LH-responsive primary aldosteronism. *J. Clin. Endocrinol. Metab.* **103**, 2926-2935 (2018).
70. Albiger, N. M. et al. A case of primary aldosteronism in pregnancy: do LH and GNRH receptors have a potential role in regulating aldosterone secretion? *Eur. J. Endocrinol.* **164**, 405-412 (2011).
71. Berthon, A., Drelon, C. & Val, P. Pregnancy, primary aldosteronism, and somatic *CTNNB1* mutations. *N. Engl. J. Med.* **374**, 1493-1494 (2016).
72. Murtha, T. D., Carling, T. & Scholl, U. I. Pregnancy, primary aldosteronism, and somatic *CTNNB1* mutations. *N. Engl. J. Med.* **374**, 1492-1493 (2016).

Acknowledgements

The *CTNNB1* plasmid was a kind gift of Mariann Bienz, Medical Research Council Laboratory of Molecular Biology, Cambridge. The project was funded in part by the British Heart Foundation through a Clinical Research Training Fellowship FS/19/50/34566 and PhD Studentship FS/14/75/31134, by the National Institute of Health Research (NIHR) through Senior Investigator award NF-SI-0512-10052, all to M.J.B., and by NIHR Efficacy and Mechanisms Evaluation Project 14/145/09 and Barts and the London Charity project MGU0360, to W.M.D. and M.J.B. The project was further funded through institutional support from INSERM, the Agence Nationale de la Recherche (ANR-15-CE14-0017-03), and the Fondation pour la Recherche Médicale (EQU201903007864) to M.-C.Z. E.A.B.A. is a Royal Society-Newton Advanced Research Fellow (NA170257/FF-2018-033). R.V.T. is supported by a Wellcome Trust Investigator Award (grant number 106995/Z/15/Z) and the National Institute for Health Research (NIHR) Oxford Biomedical Research Centre Programme. C.P.C. is supported the NIHR Biomedical Research Centre at Barts and The London School of Medicine and Dentistry. The research of J.L.K., Z.T., and R.F. was supported by the National Medical Research Council and Biomedical Research Council of Singapore. Research in London and Cambridge, UK, was further supported by the NIHR Barts Cardiovascular Biomedical Research Centre (BRC), and Cambridge BRC-funded Tissue Bank. The research utilised Queen Mary University of London's Apocrita HPC facility, supported by QMUL Research-IT (http://doi.org/10.5281/zenodo.438045). Assistance of the Endocrine Unit Laboratory of the National University of Malaysia (UKM) Medical Centre, and from Long Kha Chin and Siti Khadijah, UKM, is acknowledged.

Author Contributions

C.P.C., E.A.B.A. and M.J.B. discovered the mutations in *GNA11* and *GNAQ,* replicated by J.Z. and F.F.-R. J.Z., E.A.B.A., C.P.C., F.F.-R., S. Boulkroun, H.L.S., M.-C.Z., and M.J.B. conceived and designed the subsequent experiments/analyses. C.J., A.T., H.L.S., E.C., G.A., X.W., E.G., L.A., S. Backman, P.H., P.B., T.A., R.S., D.B., J.P.K., W.M.D., L.P. and F.K.F. contributed to cohort ascertainment, phenotypic characterization and recruitment. S. Backman, C.P.C., S.P., Z.T., L.M., T.A., and S.G. contributed to whole-exome/RNA sequencing production, validation, analysis and re-analysis. J.Z., F.F.-R., S. Boulkroun, X.W., A.E.D.T., E.A.B.A., E.C., S.G., G.A., and T.A. performed targeted sequencing and RT-PCR analyses. J.Z. performed the laser capture microdissection (LCM) and genotyping of adrenal zones and biopsy punches. S.J., S. Boulkroun, A.M. and J.Z. performed and F.F.-R. and E.A.B.A. analyzed the immunohistochemistry (IHC) staining. C.E.G S. developed antisera for use in IHC. J.Z., S.G., A.G., K.E.L., and R.V.T. contributed to the plasmid construction for *GNA11* and *GNAQ*. J.Z., E.A.B.A., and G.A. performed the functional experiments on transfected H295R and primary human adrenal cells. J.Z. and S.O. undertook confocal analyses. J.Z., E.A.B.A., F.F.-R., C.A.M., R.F., E.W., D.K., J.L.K., Z.T. and C.P.C. performed the ddPCR, WES and NGS for genotyping of adjacent adrenal regions. C.P.C., J.Z., E.A.B.A., and M.J.B. contributed to statistical analyses. E.A.B.A. and M.J.B. drafted the manuscript, for which J.Z., E.A.B.A., C.P.C., F.F.-R., S. Boulkroun, T.A., A.M., and M.J.B. contributed figures. C.P.C., F.F.-R., S. Boulkroun, M.G., V.K. and M.-C.Z. critically reviewed the text. All authors read and approved the manuscript.

Competing Interests Statement

The authors declare no competing interests.

Figure Legends

Figure 1 | Clinical and cellular schemas showing the critical roles of GNA11/Q, and their p.Gln209 residue, in the production of aldosterone. a, The renin-angiotensin-aldosterone system is superimposed on an axial PET CT image through the adrenal glands. The image is taken from the 11C-metomidate PET CT of one of the women whose unilateral (left) double-mutant aldosterone-producing adenoma (APA) was diagnosed by the scan. The hormone-enzyme, renin, is secreted from the kidneys in response to falls in blood pressure or sodium (Na^+). Its substrate, the protein angiotensinogen, is cleaved into an inert decapeptide, angiotensin 1 (Ang I), which is converted on further cleavage by the angiotensin-converting-enzyme (ACE) into the octapeptide, Ang II. This is a potent vasoconstrictor and principal physiological stimulus of aldosterone production in the zona glomerulosa cells of the outer adrenal cortex. The cellular actions of Ang II are mediated by coupling of its receptor (AT1R) to inositol trisphosphate (IP_3) and intracellular calcium (Ca^{2+}) release, through a trimeric G-protein whose α subunit is either Gα11 or Gαq. **b**, A single cell of a double-mutant APA, illustrating similar 2D and 3D-structures of GNA11/Q and GNAS, proximity of the Q209 (GNA11/Q) or Q227 (GNAS) residue to GDP, and synergism between somatic mutations of *GNA11/Q* and *CTNNB1*, upregulating luteinizing hormone and human choriogonadotrophin receptor (LHCGR) expression and production of aldosterone. The Q209 residue of Gα11 or Gαq (encoded by GNA11 or GNAQ) and analogous residue of other G-proteins is essential for GTPase activity[17]. 3D-structures for GNAQ and GNAS show the p.Gln residue in purple. Somatic or mosaic mutation of p.Gln inhibits GTPase activity and constitutively activates downstream signalling. We find that p.Gln mutation of GNA11/Q stimulates aldosterone production, and, in the adrenal, always co-exists with somatic mutation in exon 3 of *CTNNB1*. This prevents inactivation by phosphorylation (e.g. of p.Ser33, in purple, in the partial 3D sequence). Double-mutation of GNA11/Q and CTNNB1 induces high expression of multiple genes, including LHCGR, the Gαs/cyclic AMP coupled receptor of luteinizing and pregnancy hormones. The 3D structures of CTNNB1, GNAS, GNAQ, AT1-receptor, renin, ACE were downloaded from models 6M93, 3C14, 4QJ3, 6YV1, 2V0Z, 1O8A, respectively, at www.rcsb.org/.

Figure 2 | Mutations of *GNA11/Q* Q209 increase aldosterone production in human adrenocortical cells. a, Transfection of mutations of *GNA11* Q209 (Q209L, Q209P, and Q209H) into immortalized adrenocortical H295R cells stimulated aldosterone secretion (n = 40 wells examined over 5 independent experiments, $P = 1 \times 10^{-15}$ by one-way Kruskal-Wallis test, $\chi^2(4) = 105.78$). **b**, *CYP11B2* mRNA expression was increased in H295R cells transfected with *GNA11* mutations (n = 12-31 biologically independent samples, $P = 9 \times 10^{-9}$ by one-way Kruskal-Wallis test, $\chi^2(4) = 43.34$). **c**, Effect of *GNA11* mutations on aldosterone secretion in H295R cells co-transfected with either scrambled siRNA (SiScrambled) or siRNA targeting *CTNNB1* (SiCTNNB1) (n = 12-20 biologically independent samples). **d**, Effect of *GNA11* mutations on aldosterone secretion in H295R cells in the presence of the selective β-catenin inhibitor ICG-001 (3 μM) or vehicle control (n = 10 wells examined over 3 independent experiments). **e**, Cells from APA 351T, wild-type for *CTNNB1* and *GNA11*/Q (genotype presented in **Supplementary Table 2**), were transfected with either wild-type *GNA11* (WT) or *GNA11* Q209H/L only (Q209H/L) or co-transfected with either wild-type *CTNNB1* (WT + WT) or *CTNNB1* Δ45 (Δ45). Double mutations increased aldosterone secretion compared to single mutations (n = 3 independent transfections, P = 0.0003 by one-way ANOVA). **f**, Effect of *GNAQ* Q209H mutation on aldosterone secretion in H295R cells (n = 10 wells examined over 3 independent experiments). For box and whiskers plots (**a**, **b**, and **f**), the central line, box and whiskers indicate the median, interquartile range (IQR) and the 10^{th}-90^{th} percentile, respectively. For bar charts (**c** and **d**) and scatterplots (**e**), data are presented as mean values ± s.e.m. Results for **a**, **b**, **d** and **f** are expressed as fold-change from wild-type untreated transfected cells. Results for **c** and **e** are expressed as pM of aldosterone per μg of protein. The exact sample numbers (n) are as indicated below the x-axis. P-values of Dunn's multiple comparisons test are as indicated in **a** and **b**, whereas the P-values indicated in graph in **e** are of Bonferroni's multiple comparisons test. P-values indicated in **c**, **d**, and **f** are according to two-tailed Student's t-test. ns, not significant. The data used to generate these plots are provided as a Source Data file.

Figure 3 | High LHCGR expression in *GNA11/Q* and *CTNNB1* double-mutant adrenal cells. a, *LHCGR* mRNA in 10 double-mutant *CTNNB1*-mutated APAs in the discovery UK/Irish cohort was increased compared to 24 *CTNNB1*-negative APAs and 34 control adjacent adrenals ($P = 0.0001$ by one-way Kruskal-Wallis test, $\chi^2(2) = 18.02$). **b**, *LHCGR* mRNA in five double-mutant APAs in the replication French cohort was increased compared to seven APAs with solitary *CTNNB1* mutations, nine *CTNNB1* negative APAs, and six control normal adrenals ($P = 0.003$ by one-way Kruskal-Wallis test, $\chi^2(3) = 13.70$). **c**, *LHCGR* mRNA in one double-mutant APA in the replication Swedish cohort compared to two APAs with only *CTNNB1* mutations, 20 *CTNNB1*-negative APAs, and three cortisol-producing adenomas (CPA) ($P = 0.08$ by one-way Kruskal-Wallis test, $\chi^2(3) = 6.87$). **d**, LHCGR protein is highly expressed in double-mutant APAs that presented at times of high LH/HCG (e.g. patient 6 during menopause and patient 7 during pregnancy) compared to single *CTNNB1*-mutant APAs (e.g. patient F11). Scale bars, 2 mm. **e**, mRNA of *GNA11* (green symbols, $n = 6$), *CTNNB1* (magenta symbols, $n = 6$), and *LHCGR* in APA 392T cells transfected with vector control ($n = 11$), Δ45 *CTNNB1* untagged plasmid ($n = 11$), Q209P *GNA11* GFP tagged plasmid ($n = 12$), or co-transfected with both Δ45 *CTNNB1* and Q209P *GNA11* plasmids ($n = 10$). *LHCGR* mRNA was increased in double mutant cells ($P = 0.02$ by one-way Kruskal-Wallis test, $\chi^2(3) = 9.78$). The central line, box and whiskers indicate the median, IQR and the 10^{th}-90^{th} percentile, respectively. Error bars presents geometric mean ± s.d. **f**, Immunofluorescence of GNA11 (green), CTNNB1 (magenta), and LHCGR (red), of cells transfected as in **e**. Scale bars, 50 µm.**g**, Corrected Total Cell Fluorescence (CTCF) of LHCGR in cells transfected as in **e** and **f**. Double-mutant cells had higher CTCF compared to vector control ($P = 0.00005$ by one-way ANOVA). Exact *n* numbers indicated below the *x*-axis. Data presented as mean values ± s.e.m. *P*-values of Dunn's multiple comparisons test indicated in **a**, **b**, and **e** (*$P = 0.02$ comparing vector and double-mutant cells) and Holm-Sidak's multiple comparison test in **g**. *n*, represents biologically independent samples. Squares, males. Circles, females. Open symbols, fresh-frozen/RNAlater–preserved tissues. Close symbols, FFPE tissues. Red symbols, double mutants. Blue symbols, *KCNJ5* mutants. Black symbols, *KCNJ5* wild-type. The data used to generate these plots are provided as a Source Data file.

Figure 4 | Gene expression profiles in *GNA11*/*Q* and *CTNNB1* double-mutant adrenal cells. a, Heat map representation of 362 differentially expressed genes (DEG) with large variance (log_2 difference > 4) among aldosterone-producing adenomas (APA) in at least one of three transcriptome studies (2012 microarray including patient 6[5], 2015 microarray including patient 4[16], Swedish RNA-seq[19]). Each column represents the expression profile of the APA (*n* = 38). Both genes and individual APA are hierarchically clustered. The unsupervised cluster analysis of samples, indicated by the bracketing above the heat map, separated the expression profiles of *GNA11*/*Q* and *CTNNB1* double-mutant APAs (boxed red). Yellow and blue colors indicate high and low expression levels, respectively, relative to the mean (as indicated by the color scale bar). **b**, Zoomed image of the heat map in **a** of six interesting DEG (yellow arrow) that separated double-mutant (DM) APAs from single-mutant APAs (SM) and other APA genotypes. *LHCGR* (red arrow) and *CYP11B1* (black arrow) also clustered the double-mutant APAs together. **c**, The DEG highlighted in **b** were investigated in double-mutant APAs from the UK/Irish cohort compared to *CTNNB1*-negative APAs. All, except for *C9ORF84* (which had a trend), had significantly higher mRNA expression in double mutant APAs (the *P*-values indicated are according to Kolmogorov–Smirnov statistical test). **d-f**, The DEG *TMEM132E* mRNA expression was significantly higher in double mutant APAs from the UK/Irish cohort compared to *CTNNB1*-negative APAs (**d**; *P* = 0.001 by Kolmogorov–Smirnov test), in double-mutant APAs from the French cohort compared to *CTNNB1* single-mutant APAs (**e**; *P* = 0.0002 by one-way Kruskal-Wallis test, $\chi^2(2) = 13.01$; *P*-values of Dunn's multiple comparisons test are as indicated), and in *GNA11* Q209L transfected H295R cells compared to *GNA11* wild-type transfected cells (**f**; *P* = 0.001 by two-tailed Student's *t*-test). The central line, box and whiskers indicate the median, IQR and the 10th-90th percentile, respectively. *GNA11* mRNA expression in *GNA11* Q209L and wild-type transfected cells were not significantly different. The exact sample number (*n*), as indicated below the *x*-axis, represents biologically independent samples. Squares, males. Circles, females. Red symbols, double mutants. Blue symbols, *KCNJ5* mutants. Black symbols, *KCNJ5* wild-type.

Figure 5 | Aldosterone synthase (CYP11B2) and 11β-hydroxylase (CYP11B1) expression in *GNA11/Q* and *CTNNB1* double-mutant APAs. a, qPCR analysis of *CYP11B1* and *CYP11B2* mRNA expression found double-mutant APAs to have a lower *CYP11B1*:*CYP11B2* mRNA expression ratio compared to *CTNNB1* single-mutant APAs or APAs wild-type for *CTNNB1* and *GNA11/Q* (*CTNNB1*-neg APA) (P = 0.00004 by one-way Kruskal-Wallis test, $\chi^2(2) = 20.23$; P-values of Dunn's multiple comparisons test are as indicated). Results expressed as fold-change from *CTNNB1* wild-type APAs (*CTNNB1*-negative APA). Error bars presents mean ± s.e.m. The exact sample number (n), as indicated below the x-axis, represents biologically independent samples. Squares, males. Circles, females. Red symbols, double mutants. Blue symbols, *KCNJ5* mutants. Black symbols, *KCNJ5* wild-type. **b**, Immunohistochemistry of CYP11B2 and CYP11B1 in the UK/Irish cohort using the primary antibody anti-CYP11B2 #ab168388 (1:200; Abcam, UK) and anti-CYP11B1 #MABS502, clone 80-7 (1:100; Sigma-Aldrich, USA). The histotype of high CYP11B2 protein expression and low CYP11B1 expression was apparent correlating with the low CYP11B1:CYP11B2 mRNA expression seen in **a**. Scale bars, 2.5 mm.

Figure 6 | *GNA11* somatic mutations were found in the adjacent adrenals to double-mutant APAs. **a-c**, Patient 7. **d-f,** Patient 1. **a**, Genomic DNA from six different regions (R1-R6) in the fresh frozen adrenal sample and the associated RNA from regions 1-3 (R1-R3) were genotyped for *CTNNB1* and *GNA11* mutations. **b**, qPCR of samples in **a** showed 135-151 fold lower mRNA expression level of *CYP11B2* and 16,102-23,987 fold lower mRNA expression level of *LHCGR* in R1 cDNA compared to R2 and R3, respectively. Differentially expressed genes (DEG) highly expressed in double-mutant APAs but lowly expressed in R1 cDNA are presented in **Supplementary Figure 6a**. **c**, Sanger sequencing of samples in **a** detected solitary *GNA11* Q209H mutation in R1 cDNA and double *CTNNB1* S45F and *GNA11* Q209H mutations in R2 and R3 cDNA. Interestingly, genotyping of R1 genomic DNA (from the exact same sample as R1 cDNA) detected a homozygous *GNA11* Q209H mutation (**Supplementary Fig. 6a**). **d**, Patient 1 was found to have hyperplastic zona glomerulosa (ZG) in adrenal adjacent to double-mutant APA. ZG hyperplasia was demarcated by lack of subcapsular CYP11B1 (visualized using a custom antibody). The hyperplastic ZG was CYP11B2 negative (visualized using a custom antibody) while LHCGR positive (visualized using the antibody NLS1436; 1:200; Novus Biologicals, UK). This phenotype is consistently present in the UK/Irish discovery cohort (**Supplementary Fig. 5c**). **e**, Genomic DNA from the hyperplastic ZG of nine distinct regions of patient 1's adjacent adrenal were collected systematically using segmental laser capture microdissection (LCM) of formalin-fixed paraffin embedded adrenal sections stained with cresyl violet. **f**, Solitary heterozygous and solitary homozygous *GNA11* Q209P somatic mutations were detected in LCM ZG gDNA collected in **e** from regions 1 (ZG1 genomic DNA) and 6 (ZG6 genomic DNA), respectively. ZG samples from other regions were wild-type for both *CTNNB1* and *GNA11* along with the other adrenal zones (**Supplementary Fig. 6b**).

Table 1 | Clinical, biochemical, and *GNA11/Q* genotype findings in the discovery cohort of 10 UK/Irish PA patients with *CTNNB1*-mutant APAs

Somatic mutations of *CTNNB1* and *GNA11* in the UK/Irish discovery cohort were detected in patients 1, 2, and 3 by WES of APAs from 41 PA patients. Patients 4-6 are the three previously reported women[16], with patient 4's somatic mutation of *CTNNB1* detected in our first WES[4].

Patient ID	Sex	Age at surgery	Onset presentation	Tumor genotype		Measurements pre-adrenalectomy					Measurements post-adrenalectomy				
				CTNNB1	*GNA11/Q*	SBP	DBP	Plasma renin	Aldosterone	Serum potassium	SBP	DBP	Plasma renin	Aldosterone	Serum potassium
						mmHg	*mmHg*	*mU/liter*	*pmol/liter*	*mmol/liter*	*mmHg*	*mmHg*	*mU/liter*	*pmol/liter*	*mmol/liter*
					GNA11										
1	Male	12	Puberty	S45F	Q209P	180	120	<2	1,358	2.7	110	75	7	74	4.2
2	Female	35	Pregnancy	S45P	Q209P	155	85	<2	559	2.6	123	76	16	283	4.0
3	Female	20	Pregnancy	T41A	Q209H	215	120	<2	1,330	2.5	121	68	N/A	N/A	N/A
4	Female	34	Pregnancy	S33C	Q209H	190	100	<2	2,885	2.0	111	69	31	250	4.1
5	Female	26	Pregnancy	S45F	Q209H	140	86	<2	2,590	2.0	120	70	N/A	N/A	N/A
6	Female	52	Menopause	G34R	Q209P	190	100	<2	672	3.1	118	79	9.0	158	4.1
7	Female	39	Pregnancy	S45F	Q209H	160	101	<2	2,382	2.5	120	83	16.1	124	4.7
8	Female	41		S45F	Q209P	160	90	<2	480	3.2	101	65	91	236	4.5
					GNAQ										
9	Female	23	Pregnancy	G34E	Q209H	167	114	<2	2000	3.3	121	85	N/A	N/A	N/A
10	Female	26	Pregnancy	G34R	Q209L	170	110	<2	603	4.1	123	78	14	408	4.7

N/A, not available. SBP, systolic blood pressure. DBP, diastolic blood pressure. Units of measurements pre- and post-adrenalectomy are shown in italics. Bold denotes the name of the gene (*GNA11*/*GNAQ*) in which the Q209 mutation was found.

730 **Table 2 | Clinical presentation and genotype of *GNA11/Q/S* in the APA of 17 primary aldosteronism patients who had *CTNNB1*-mutant APAs from the**
731 **replication cohorts**

Replication cohort	Patient ID	Sex	Age PA	Hypertensive at pregnancy (number of pregnancies)	Tumor genotype						
					CTNNB1 genotype	*GNA11* Q209	*GNA11* R183	*GNAQ* Q209	*GNAQ* R183	*GNAS* Q227	*GNAS* R201
French cohort	F1	Female	29	Yes (1)	S45F	WT	WT	WT	WT	WT	WT
	F2	Male	40	-	S45P	WT	WT	WT	WT	WT	WT
	F3	Female	35	No (2)	S37C	WT	WT	WT	WT	WT	WT
	F4	Male	33	-	S45A	WT	WT	WT	WT	WT	WT
	F5	Female	43	No (1)	S45F	Q209P	WT	WT	WT	WT	WT
	F6	Female	45	Yes (2)	S45P	WT	WT	WT	WT	WT	WT
	F7	Female	55	N/A	S45P	WT	WT	WT	WT	WT	WT
	F8	Female	55	N/A	S45P	WT	WT	WT	WT	WT	WT
	F9	Female	26	Yes* (1)	S37P	WT	WT	Q209H	WT	WT	WT
	F10	Female	51	Yes (1)	S45P	Q209H	WT	WT	WT	WT	WT
	F11	Male	36	-	S45P	WT	WT	WT	WT	WT	WT
	F12	Female	56	No (10)	D32Y	Q209H	WT	WT	WT	WT	WT
	F13	Female	56	No (0)	S45Y	WT	WT	WT	WT	WT	WT
	F14	Female	17	No[#] (0)	G34V	WT	WT	Q209H	WT	WT	WT
Swedish cohort	S1	Female	55	Yes[†] (2)	S45P	WT	WT	Q209H	WT	WT	WT
	S2	Female	59	N/A	S45P	WT	WT	WT	WT	WT	WT
	S3	Female	26	N/A	S37F	WT	WT	WT	WT	WT	WT

PA, primary aldosteronism. N/A, not available. WT, wild-type. *pre-eclampsia. #hypertensive at puberty. †onset at age 24 years old preceding first pregnancy.

Online Methods

Patient cohorts. All patients were confirmed to have primary aldosteronism by raised aldosterone/renin ratio, positive confirmatory tests and lateralization studies (CT/PET CT[73], MRI and AVS) according to the institutional protocols at the various centres and in accordance with the Endocrine Society guidelines[74,75]. All patients gave written informed consent for genetic and clinical investigation according to local ethics committee guideline (Cambridgeshire Research Ethics Committee for Addenbrooke's Hospital, University of Cambridge or the Cambridge East Research Ethics Committee for St Bartholomew's Hospital, Queen Mary University of London for the UK cohort; Assistance Publique-Hôpitaux de Paris Research Ethics Committee for the French cohort; Regional Ethical Review Board in Uppsala for the Swedish cohort).

UK/Irish cohort. The seven patients with double-mutations of *CTNNB1* and *GNA11* were among 117 UK/Irish patients who were investigated at St Bartholomew's Hospital, London or Addenbrooke's Hospital, Cambridge, or whose operative specimen was received for investigation, during the period 2004 to 2017.

French cohort. Patients with primary aldosteronism were recruited between 1999 and 2016 within the COMETE (COrtico- et MEdullo-surrénale, les Tumeurs Endocrines) network (COMETE-Hôpital Européen Georges Pompidou protocol authorization CPP 2012-A00508-35). 198 patients were screened for *CTNNB1* mutations. For some of the patients included in this study, the genetic screening of mutations in *KCNJ5*, *ATP1A1*, *CACNA1D* and *ATP2B3* was previously described[27,76].

Swedish cohort. 15 tumors were selected from a previously documented international cohort[19,77]. Adrenal specimens were collected from 348 patients from centres in Sweden, Germany, France and Australia.

Whole exome sequencing (WES). WES of 40 pairs of APAs and adjacent adrenal from UK patients was conducted in the Barts and London Genome Centre, and the Cardiovascular Research Institute of the University of Singapore, with overlap of eight pairs of samples, and previously genotyped controls (*n* = 3 in each centre/institute) as validation of sensitivity (not included in analysis). The 41st APA was analyzed together with germline DNA from blood processed commercially by GATC Biotech, Germany. MuTect2 analysis was conducted in order to identify adrenocortical genes with somatic mutations, predicted by Sorting Intolerant from Tolerant (SIFT) and Polymorphism Phenotyping (PolyPhen)-2 to be functional. Candidate mutations were confirmed by Sanger sequencing of DNA from fresh samples of the APA, and sought in other previously genotyped APAs that were not included in the WES.

Quality control of WES samples. Genomic DNA of samples was quality assessed by gel electrophoresis, Agilent 2200 Tapestation and Genomic DNA screentape (Agilent Technologies, Waldbronn, Germany), or as per GATC Biotech standard protocol. Samples with low degradation and a majority of high molecular weight were taken forward for WES.

WES of patient 1. WES using the Illumina HiSeq 2000 Sequencer was conducted on DNA extracted from the APA along with the paired germline DNA extracted from the venous blood (samples processed commercially by GATC Biotech, Germany). WES samples were prepared as an Illumina sequencing library and the sequencing libraries were enriched using the Agilent SureSelectXT Human All Exon V6 Kit. The captured libraries were sequenced and downstream analysis conducted as described below.

WES of patient 2. WES using the Illumina NextSeq 500 Sequencer was conducted on genomic DNA extracted from APAs from 21 PA patients along with paired adjacent normal adrenal and APAs from three primary aldosteronism patients with known genotype (as sensitivity controls). 50 ng of each DNA sample was processed using the Nextera Rapid Capture Enrichment kit, with the Coding Exome Oligo (CEX) pool. Tagmented DNA was assessed using the Agilent 2200 Tapestation in conjunction with the HSD1000 screentape. All samples showed expected fragmentation profiles with an average fragment

782 size of 300 bp. Enriched libraries were validated using the Agilent 2200 Tapestation in conjunction with
783 the D1000 screentape. Equimolar amounts of each sample library were pooled together for sequencing
784 which was carried out using the llumina NextSeq®500 high-output kit.

785 *WES of patient 3.* WES using the Illumina Hiseq 2500 sequencer was conducted on genomic DNA
786 extracted from 27 APAs along with paired adjacent normal adrenal and three APAs with known
787 genotype (as sensitivity controls). 1 µg of genomic DNA was fragmented using sonication (Covaris,
788 S220), optimized to give a distribution of 200-500 bp that was verified using a 2100 Bioanalyzer (Agilent,
789 G2939BA). Library preparation was carried out using Kapa DNA HTP Library Preparation Kit (KAPA
790 Biosystems, 07 138 008 001). Hybridization of adapter ligated DNA was performed at 47 °C, for 64 to 72
791 h, to a biotin-labelled probe included in the Nimblegen SeqCap EZ Human Exome Kit (Roche,
792 06465692001). Libraries were sequenced using the Illumina Hiseq 2500 sequencing system and paired-
793 end 101-bp reads were generated for analysis with 100x coverage per sample.

794 *WES data analysis.* Variant calling was performed using Burrows-Wheeler Aligner (BWA) v.
795 0.7.12 (for 341T) or v. 0.7.15 to align raw reads in the FASTQ files to human reference genome GRCh37.
796 The alignments were sorted and marked for PCR duplicates using Picard Tools software v.1.119 (for
797 341T) or v.1.7. This was followed by base quality score recalibration (BQSR) using the genome analysis
798 toolkit (GATK) for tuning the quality scores to reflect higher accuracy of base qualities. For 341T, ContEst
799 from GATK was used to calculate cross-sample contamination between samples, using blood as the
800 "normal" versus each of the APA samples. A panel of normals was created from the blood sample of the
801 boy using dbSNP and COSMIC as reference. In order to enrich the panel of normals, we utilize WES of 11
802 other blood samples, all pre-processed using the same protocol as described above. Resulting BAMs
803 were analyzed with GATK MuTect v.2 software to identify somatic variants. Normal and tumor pairs
804 were analyzed together when available. For tumor-only samples, the MuTect tumor-only algorithm was
805 used. The contamination estimates derived from ContEst, and the dbSNP, COSMIC, the blood sample
806 and the panel of normals were used as resources in the input parameters to filter variants observed in

807 the germline samples. SNPs, with a threshold coverage of at least 10 reads on the respective nucleotide,
808 were assessed. Oncotator was used to annotate the variants passing the filters
809 (http://www.broadinstitute.org/oncotator).

810

811 **Re-analysis of RNA-seq data of Swedish cohort.** RNA sequencing previously described in Backman et
812 al.[19] was used for variant identification and analysed for gene expression differentiation.

813 *RNA-seq variant detection.* RNA-seq variant detection was performed following the
814 recommendations on the GATK workflow for RNA-seq variant discovery. RNA-seq reads were aligned to
815 the UCSC hg19 reference genome using the STAR 2-pass method for sensitive novel junction discovery.
816 Picard tools software (picard-tools-1.119) was then used to sort and mark PCR duplicates on the
817 alignments. The SplitNCigarReads function from GATK was used to reformat alignments, by splitting
818 reads into exon segments, and to reassign reads with good mapping quality into a GATK format. We
819 performed an indel realignment step followed by the quality score recalibration protocol. Variants were
820 called using the HaplotypeCaller from GATK using the '–dontUseSoftClippedBases' parameter and
821 setting the minimum phred-scaled confidence threshold to 20 (-stand_call_conf 20.0). The following
822 hard filters were applied to the called variants: '-window 35 -cluster 3 -filterName FS -filter "FS > 30.0" -
823 filter Name QD -filter "QD < 2.0"'. Variant annotation was performed using ANNOVAR.

824 *Comparison of CTNNB1-only mutants with double-mutants.* Gene expression differentiation of
825 the three samples with the *CTNNB1* mutation was performed as follows. RNA-seq fastq files were
826 pseudo-aligned to the human GRCh37 cDNA reference sequences from ENSEMBL using kallisto v0.46.0.
827 Transcript abundance was quantified using the kallisto 'quant' function with default settings. Gene
828 expression analysis was performed with DESeq2 (v1.24.0). Genes with less than 10 reads were removed
829 from further analysis. Dispersion estimates and size factors were calculated using all 15 samples, with
830 gender as a covariate in the design matrix. The two single-mutation samples were then compared to the
831 sample with a double-mutation.

Sanger sequencing of *CTNNB1* and *GNA11/Q/S.* *Laser capture microdissection (LCM) of adrenal zones.* Freshly sectioned 10 µm FFPE adrenal sections of patient 1 were used for LCM. Serial adrenal sections were fixed and rehydrated in ethanol then stained by cresyl violet (Sigma-Aldrich, USA) for 1 min. The sections were then dehydrated in ethanol and cleaned in Histo-clear II (AGTC Bioproducts Ltd, UK). After fixing and staining the adrenal sections, ZG cells were collected by LCM technique using a Zeiss PALM Microbeam laser microdissection system (Carl Zeiss Microscopy, USA) with PALMRobo v4.3 software according to the manufacturer's instructions. All the pooled ZG LCM samples collected from the same area of adrenal sections were then stored at -20 °C until RNA and genomic DNA extraction.

Nucleic acid extraction. Genomic DNA (gDNA) from fresh frozen/RNAlater solution–preserved tissue samples was extracted using Reliaprep™ gDNA Tissue miniprep system (Promega, USA). gDNA from FFPE samples collected by LCM were extracted using Arcturus® PicoPure® DNA Extraction Kit (Applied Biosystems™, USA). gDNA of blood from patient 1 and patient 7 were extracted using Nucleon™ BACC3 Genomic DNA Extraction Kit (GE Healthcare Life Sciences, UK) according to manufacturer's recommendation.

For the UK/Irish cohort, total DNA-free RNA was isolated from fresh frozen/RNAlater solution–preserved samples using TRIzol (Ambion Life Technologies, Carlsbad CA) and PureLink® RNA Mini Kit (Invitrogen™, USA) according to manufacturer's recommendation. The PureLink® DNase Set was used in combination to remove DNA from RNA (Invitrogen, USA) by on-column digestion. If the fresh frozen/RNAlater solution–preserved samples were not available, total RNA and gDNA were extracted from FFPE tissue samples blocks using AllPrep DNA/RNA FFPE Kit (Qiagen, USA) according to manufacturer's recommendation (FFPE extracted DNA/RNA is reported when used). This kit is also used on fresh frozen samples when RNA and gDNA from the same sample were required. Total RNA from FFPE samples collected by LCM were extracted by Arcturus™ Paradise™ Plus RNA Extraction and Isolation Kit (Applied Biosystems™, USA) in combination with the PureLink® DNase Set, according to

manufacturer's recommendation. After extraction reverse transcription was performed using the High Capacity RNA-to-cDNA kit (Fisher Scientific, USA) according to manufacturer's instructions. The cDNA was purified by DNAclear™ Purification Kit (Invitrogen™, USA).

For the French cohort, total RNA was extracted using Janke and Kunkel's Ultra-Turrax T25 (IKA technologies, Staufen DE) in Trizol reagent (Ambion Life Technologies, USA) according to the manufacturer's recommendations. After deoxyribonuclease I treatment (Life Technologies, USA), 500 ng of total RNA were retro-transcribed (iScript reverse transcriptase, Bio-Rad, USA).

PCR and sequencing of *CTNNB1* and *GNA11/Q/S.* Primers used for *CTNNB1*, *GNA11*, *GNAQ* and *GNAS* amplification in gDNA and cDNA samples are described in **Supplementary Tables 5** and **6** or as previously described[16,76]. For UK/Irish cohort, PCR was performed on 100 ng of DNA in a final volume of 20 µl reaction using AmpliTaq Gold™ Fast PCR Master Mix (Thermo Fisher, USA) according to manufacturer's instructions. Sanger sequencing of PCR products was performed using LIGHTRUN Tube sequencing service from Eurofins (Germany). For the French cohort, PCR was performed on 100 ng of DNA in a final volume of 25 µl containing 400 nM of each primer, 200 µM deoxynucleotide triphosphate and 1.25 U Taq DNA Polymerase (Sigma-Aldrich, USA). Sanger sequencing of PCR products was performed using the Big Dye TM Terminator v3.1 Cycle Sequencing Kit (Applied Biosystems, USA) on an ABI Prism 3700 DNA Analyzer (Applied Biosystems, USA). Sanger Sequencing alignment was performed using GATC Viewer 1.00 or BioEdit version 7.2.5.

Droplet digital PCR (ddPCR) of *GNA11/Q.* Specific droplet digital PCR (ddPCR) assays for *GNA11* (c.627 A>C, c.627 A>T, and c.626A>C) and *GNAQ* (c.627A>C and c.627A>T) mutation detection were designed on the Bio-Rad's Digital Assay Site. Each ddPCR reaction mixture (20 µL) contained 45 ng of DNA template, 1 µL of 20X WT (HEX) and mutant (FAM) assays, 4U of restriction enzyme HindIII (New England Biolabs), and 10 µL of 2X Bio-Rad ddPCR Supermix. The reaction mixture was mixed with 70 µL Bio-Rad droplet generator oil and partitioned into 15,000–20,000 droplets by using the QX-100 droplet

generator (Bio-Rad), and transferred to a 96-well PCR reaction plate. PCR conditions were 10 min at 95 °C, 40 cycles of denaturation for 30 s at 94 °C and extension for 60 s at 57 °C with ramp rate of 2.5 °C/s, followed by 10 min at 98 °C. The plate was then transferred to the QX-100 droplet reader (Bio-Rad). QuantaSoft software version 1.3.2.0 (Bio-Rad) was used to quantify the copies of target DNA. The ratio of positive HEX and positive FAM events was used to identify the presence and the proportion of target mutations.

NGS targeted sequencing of *CTNNB1* and *GNA11/Q/S.* *French centre.* Immunohistochemistry-guided next generation sequencing (CYP11B2 IHC-guided NGS) was performed as previously described[8]. Before DNA extraction from FFPE tissue, APA was identified by CYP11B2 IHC and the areas of interest were delimited and isolated for DNA extraction by scraping unstained FFPE sections guided by the CYP11B2 IHC slide using a scalpel under a Wild Heerbrugg or Olympus microscope. DNA was extracted from FFPE sections using the AllPrep DNA/RNA FFPE kit (Qiagen). NGS was performed using an amplicon based NGS kit on an Illumina MiSeq sequencer as previously described[78].

British centre. Assays were designed using Primer3 and 5' tagged with Fluidigm TSP sequences to allow barcoding and adapter addition. Samples were PCR amplified with FastStart High Fidelity (Roche) with cycling conditions 95 °C, 2 min, 35 cycles (95 °C, 30 s; 55 °C, 30 s; 72 °C, 30 s), and 72 °C for 5 min on an MJ tetrad MJ225. PCRs were checked on 2% agarose gel. 1 ml of a 1 in 100 dilution of PCR product was used in a second round of PCRs to add Barcodes and Illumina adapters with cycling conditions 95 °C, 10 min, 15 cycles (95 °C, 30 s; 60 °C, 30 s; 72 °C, 30 s), and 72 °C for 3 min on an MJ tetrad MJ225. Products were quantified by Qubit and loaded onto an Illumina NextSeq 500 to generate in excess of 1,000x 75-bp paired end reads. Reads were aligned to human hg38 using BWA and BAM files visualized in IGV.

WES for validation. WES was performed for validation for some samples listed in **Supplementary Table 4**. Using the Illumina Hiseq 4000 sequencer was conducted on genomic DNA. 1 µg of genomic DNA was fragmented using sonication (Covaris, S220), optimized to give a distribution of 200-500 bp that was verified using a 2100 Bioanalyzer (Agilent, G2939BA). Library preparation was carried out using Kapa DNA HTP Library Preparation Kit (KAPA Biosystems, 07 138 008 001). Hybridization of adapter ligated DNA was performed at 47 °C, for 64 to 72 h, to a biotin-labelled probe included in the Nimblegen SeqCap EZ Human Exome Kit (Roche, 06465692001). Libraries were sequenced using the Illumina Hiseq 4000 sequencing system and paired-end 150-bp reads were generated for analysis with 200x coverage per sample. Exome data were analyzed using GATK v3.7 with the human_g1k_v37_decoy as reference genome. Annotation of variants was performed using annovar (version 10-24-2019) and in-house pipelines.

Functional analyses in human adrenocortical cells. *Construction of wild-type and mutant vectors.* *GNA11* wild-type and Q209L plasmids was kindly given by Rajesh V. Thakker (University of Oxford), constructed in a pBI-CMV2 vector. *CTNNB1* wild-type and del45 (*CTNNB1* Δ45) plasmids were kindly given by Mariann Bienz (University of Cambridge), constructed in a pcDNA3 vector. *GNA11* Q209H and Q209P were generated using the NEB Q5® Site-Directed Mutagenesis Kit (New England Biolabs, UK) using the following primers in **Supplementary Table 7** according to the manufacturer's recommendation.

Functional assays in H295R and primary human adrenal cells. The human adrenocortical carcinoma cell line H295R and primary human adrenal cells were cultured as previously described[16]. H295R cells and primary human adrenal cells were transfected with pBI-CMV2 empty vector, *GNA11* wild-type, *GNA11* Q209H/L/P plasmids, with/or without the co-transfection of *CTNNB1* wild-type, *CTNNB1* Δ45 plasmids by electroporation using the Neon™ Transfection System 10/100 µL Kit (Invitrogen™, USA).

For H295R cells, 48 h after transfection, the culture medium was replaced with serum free medium with or without 10 nM angiotensin II (Ang II) or 3 or 10 µM of the CTNNB1 inhibitor ICG-001 (AdooQ BioScience, USA). Supernatant was collected for aldosterone measurement after 24 h and cells were harvested for mRNA expression analysis and protein quantification. For primary adrenal cells, supernatant was collected for aldosterone measurement at 24, 27 (+3), 30 (+6) and 48 (+24) h post-transfection and cells were harvested for mRNA expression analysis and protein quantification at the last time point (48 h post-electroporation). All cells harvested for mRNA expression analysis was kept at -80 °C in Trizol until batch extraction of nucleic acid and protein.

Aldosterone and cortisol measurement. Aldosterone secretion of primary human adrenal cells was measured using the Homogeneous Time Resolved Fluorescence (HTRF®) Aldosterone competitive assay (Cisbio, France) according to manufacturer's recommendation. Aldosterone secretion was measured on the IDS-iSYS Automated System (#IS-3300, Immunodiagnostic Systems, Germany) for H295R cells at the National University of Malaysia and by Aldosterone HTRF kit (#64ALDC0A, Cisbio, France) using FLUOstar Omega plate reader (BMG labtech) at Queen Mary University of London for primary adrenal cells. The cortisol levels were measured using ECLIA-Technology (Cobas e411, Roche, Germany) and immunoassay for the in vitro quantitative determination of cortisol (#06687733 190, Roche, Germany). Aldosterone and cortisol results were normalized by protein amount estimated by Pierce BCA Protein Assay Kit (Thermo Fisher Scientific, USA) according to manufacturer's recommendation.

RT-qPCR analyses. *RT-qPCR analysis of the UK/Irish Cohort and adrenocortical cells.* mRNA expression of genes of interest was quantified using commercially available TaqMan gene expression probes (Thermo Fisher Scientific, USA) listed in **Supplementary Table 8**. The RT-qPCR was performed using the C1000 Touch Thermal Cycler machine (Bio-Rad, USA) or the 7000 SDS (Applied Biosystems, USA) according to

manufacturer's recommendation. Results were analysed using the $2^{-\Delta\Delta CT}$ method using the housekeeping 18S rRNA (Thermo Fisher Scientific, USA) for normalization.

RT-qPCR analysis of APAs from the French cohort. Primers used for *LHCGR*, *CYP11B1* and *CYP11B2* RT-qPCR are described in **Supplementary Table 9**. RT-qPCR was performed using SsoAdvanced Universal SYBR Green Supermix (Bio-Rad, USA) on a Bio-Rad C1000 touch thermal cycler (CFX96 Real Time System) according to the manufacturer's instructions. CFX Manage TM Software v3.1 (Bio-Rad, USA) was used for qPCR data acquisition. Normalization for RNA quantity and reverse transcriptase efficiency was performed against three reference genes (geometric mean of the expression of Ribosomal *18S* RNA, *GAPDH* and *HPRT*; primers are described in **Supplementary Table 9**), in accordance with the MIQE guidelines[79]. Quantification was performed using the standard curve method. Standard curves were generated using serial dilutions from a cDNA pool of all samples. Fold change over control adrenals excised from patients who had undergone enlarged nephrectomies for renal carcinoma (*LHCGR* RT-qPCR) and over non-*CTNNB1* mutated APA (*CYP11B1* and *CYP11B2* RT-qPCR) were then calculated.

Protein expression analyses. *Immunohistochemistry (IHC).* The primary antibodies used for IHC are as follows: anti-LHCGR #NLS1436 (1:200; Novus Biological, USA), anti-CYP11B1 (1:100) and anti-CYP11B2 (1:100) gifted by Celso E. Gomez-Sanchez[78], two commercial anti-CYP11B2 #ab168388 (1:200; Abcam, UK) and #MABS1251 (1:2,500; Sigma-Aldrich, USA), and one commercial anti-CYP11B1 #MABS502 (1:100; Sigma-Aldrich, USA). The secondary antibodies used in the IHC are as follows: affinity purified goat anti-rabbit antibody for LHCGR antibody #BA-1000 (1:400; Vector laboratories, USA), affinity purified horse anti-mouse antibody for CYP11B2 antibody #BA-2000 (1:400; Vector Laboratories, USA), and affinity purified rabbit anti-rat antibody for CYP11B1 antibody #BA-4001 (1:400; Vector Laboratories, USA).

Immunofluorescence (IFC). 48 h after electroporation, transfected H295R and primary human adrenal cells were processed for IFC as previously described[16]. Cells were incubated with anti-LHCGR

#NLS1436 (1:200; Novus Biologicals, UK) and anti-CTNNB1 #610154 (1:100; BD transduction Lab, USA) at room temperature for 1 h and then with goat anti-rabbit IgG (H+L) cross-adsorbed secondary antibody, Alexa Fluor 568 (A-11011, 1:1000; Invitrogen, USA) and goat-anti-mouse IgG (H+L) cross-adsorbed secondary antibody, Alexa Fluor 647 (A-21235, 1:1000; Invitrogen, USA) at room temperature for 1 h. Immunofluorescence was visualized using a Zeiss LSM 710 (for ADR351T and 357T)/880 (for ADR392T) confocal microscopes. A second set of primary antibodies, a combination of anti-LHCGR #NBP2-52504 (1:100; Novus Biologicals, UK) and anti-CTNNB1 #71-2700 (1:100; Thermo Fisher Scientific, USA) was used for validation of first set of primary antibodies used. For the second set of primary antibodies, Alexa Fluor 405 (A-31553, 1:1,000; Invitrogen, USA), Alexa Fluor 647 (A-21235, 1:1,000; Invitrogen, USA) and Alexa Fluor 568 (A-11011, 1:1,000; Invitrogen, USA) were used as the secondary antibodies. Zen Blue 21 Edition software (Zeiss, Germany) was used for confocal microscopy image acquisition. Quantification of immunofluorescence was performed using (Fiji Is Just) ImageJ v1.52e Java 1.8.0_66 as published online (Fitzpatrick, M. Measuring cell fluorescence using ImageJ. *The Open Lab Book. https://theolb.readthedocs.io/en/latest/imaging/measuring-cell-fluorescence-using-imagej.html*). Cells successfully transfected with Δ45 *CTNNB1* was defined based on having a corrected total cell fluorescence (CTCF) for CTNNB1 >100,000.

Statistical analysis. All parametric data are presented as mean ± s.e.m. For non-parametric data, results were presented as median ± 95% confidence interval or as geometric mean ± 95% confidence interval (for qPCR data only). For parametric data, two-tailed Student's *t*-test and one-way or two-way ANOVA statistical tests were performed depending on the grouping factors. Kolmogorov-Smirnov test (when comparing 2 groups) or Kruskal-Wallis test (when comparing >2 groups) was used for non-parametric data. Tests for normality/lognormality and adjustment for multiple comparisons were performed. All the analysis was performed using GraphPad Prism software (version 7.04 and version 9.0.1) or Microsoft Excel v.2016 (for Student's *t*-test). *P*-values lower than 0.05 were considered statistically significant.

Data Availability Statement

Source data for **Figure 2a**-**f** and **Figure 3a**-**c**,**e**,**g** are provided with the paper. The raw RNA-seq dataset analyzed to generate **Figure 4a,b**, **Supplementary Table 3** and **Supplementary Figure 4** is available upon requests to the Science for Life Laboratory Data Centre through the DOI link https://doi.org/10.17044/NBIS/G000007. Regulations by the service provider may make access technically restricted to PIs at Swedish organizations. The microarray datasets analyzed to generate **Figure 4a,b** are deposited in the Gene Expression Omnibus database (GSE64957) or are available from the corresponding author on reasonable request. The whole exome sequencing raw data of the 41 APAs and controls investigated for recurrent pathogenic somatic mutation are available from the Sequence Read Archive (SRA) under the accession numbers PRJNA732946 and PRJNA729738. All other raw data that support the findings of this study are available from the corresponding author upon reasonable request.

Methods-only References

73. Burton, T. J. et al. Evaluation of the sensitivity and specificity of (11)C-metomidate positron emission tomography (PET)-CT for lateralizing aldosterone secretion by Conn's adenomas. *J. Clin. Endocrinol. Metab.* **97**, 100-109 (2012).

74. Letavernier, E. et al. Blood pressure outcome of adrenalectomy in patients with primary hyperaldosteronism with or without unilateral adenoma. *J. Hypertens.* **26**, 1816-1823 (2008).

75. Funder, J. W. et al. Case detection, diagnosis, and treatment of patients with primary aldosteronism: an endocrine society clinical practice guideline. *J. Clin. Endocrinol. Metab.* **93**, 3266-3281 (2008).

76. Fernandes-Rosa, F. L. et al. Genetic spectrum and clinical correlates of somatic mutations in aldosterone-producing adenoma. *Hypertension* **54**, 354-361 (2014).

77. Akerstrom, T. et al. Comprehensive re-sequencing of adrenal aldosterone producing lesions reveal three somatic mutations near the KCNJ5 potassium channel selectivity filter. *PLoS One* **7**, e41926 (2012).

78. Gomez-Sanchez, C. E. et al. Development of monoclonal antibodies against human CYP11B1 and CYP11B2. *Mol. Cell. Endocrinol.* **383**, 111-117 (2014).

79. Bustin S. A. Why the need for qPCR publication guidelines? The case for MIQE. *Methods* **50**, 217-226 (2010).

Figure 1 (a-b)

Clinical (a) and cellular (b) schemas showing the critical roles of GNA11/Q, and their p.Gln209 residue, in the production of aldosterone.

a.

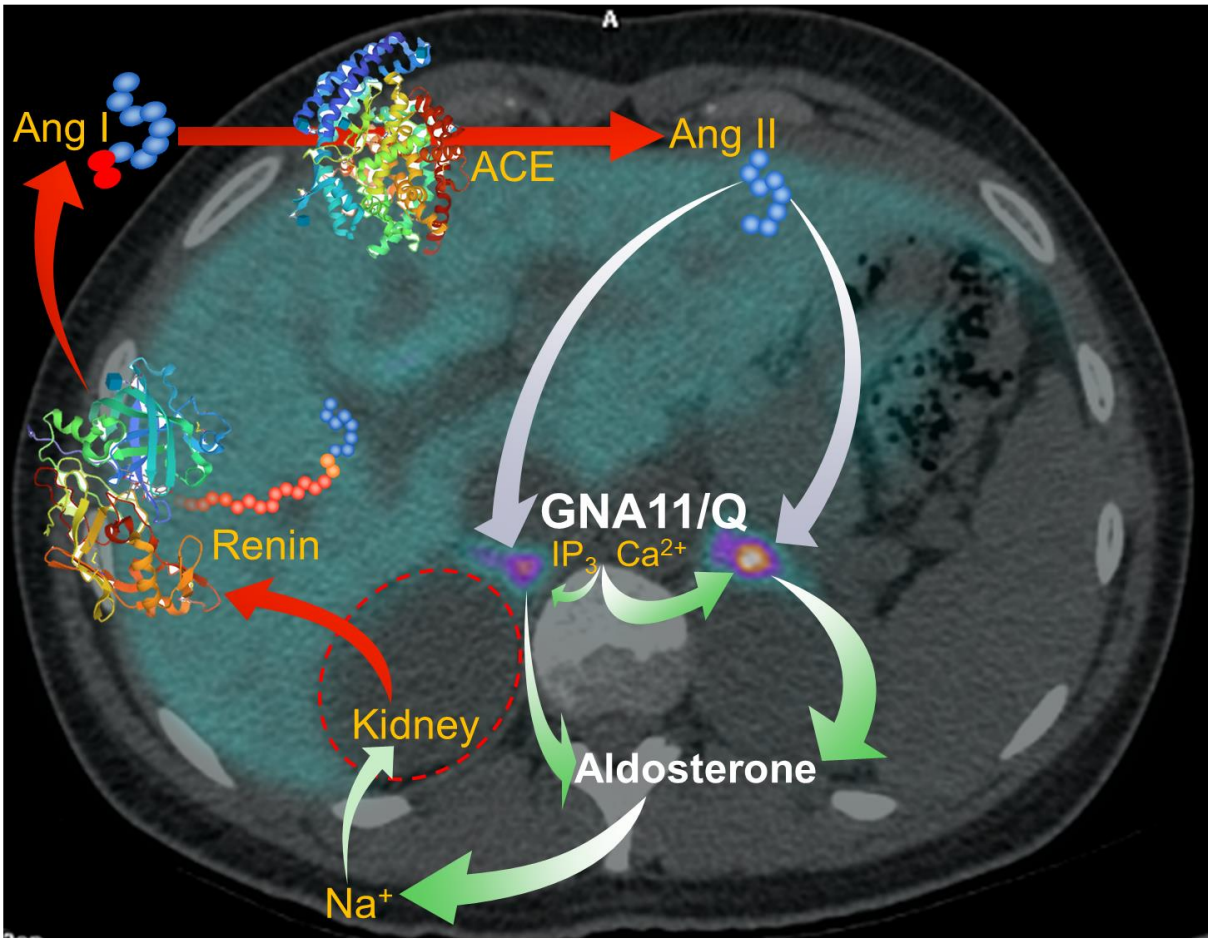

b.

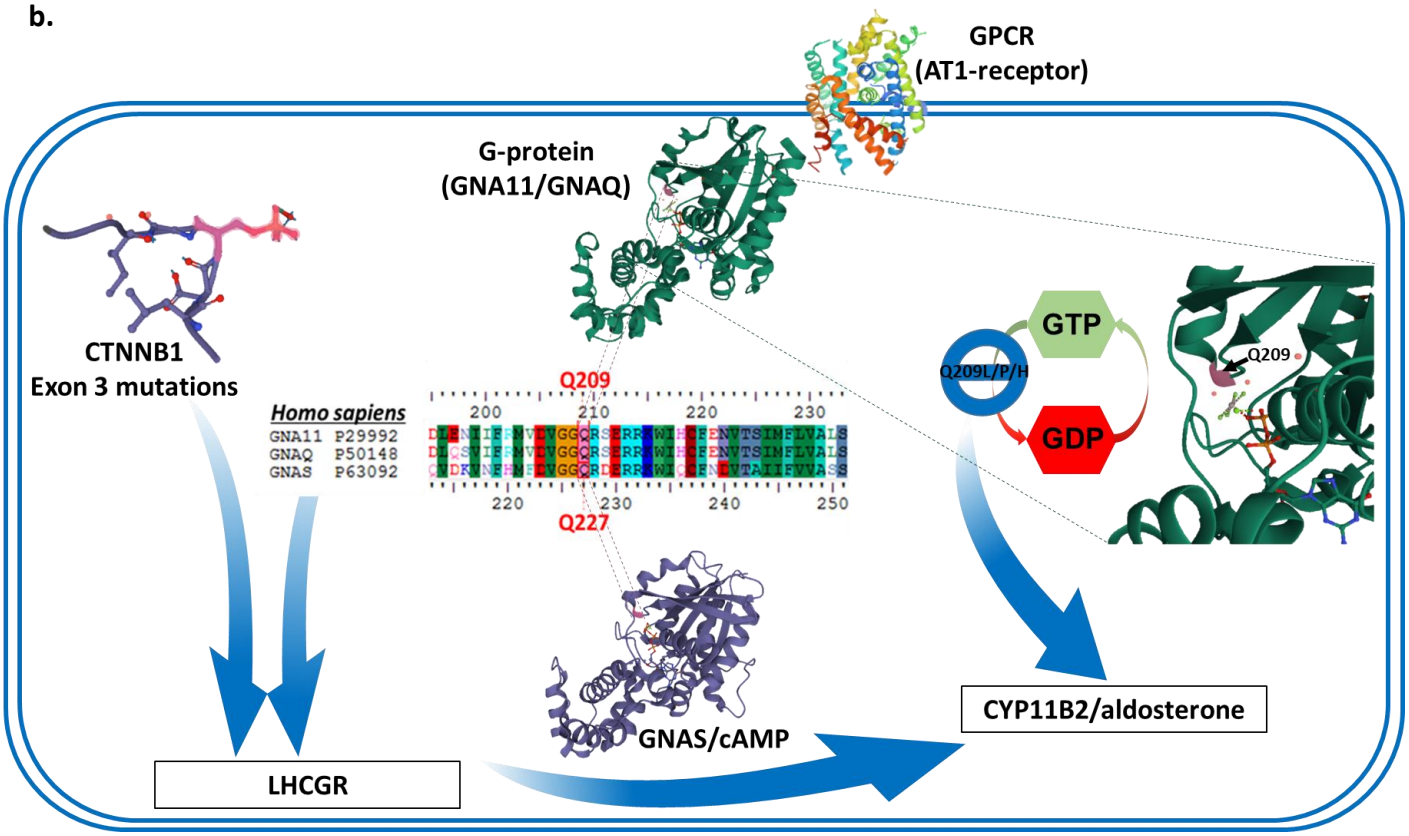

Figure 2 (a-f)

Mutations of *GNA11/Q* Q209 increase aldosterone production in human adrenocortical cells.

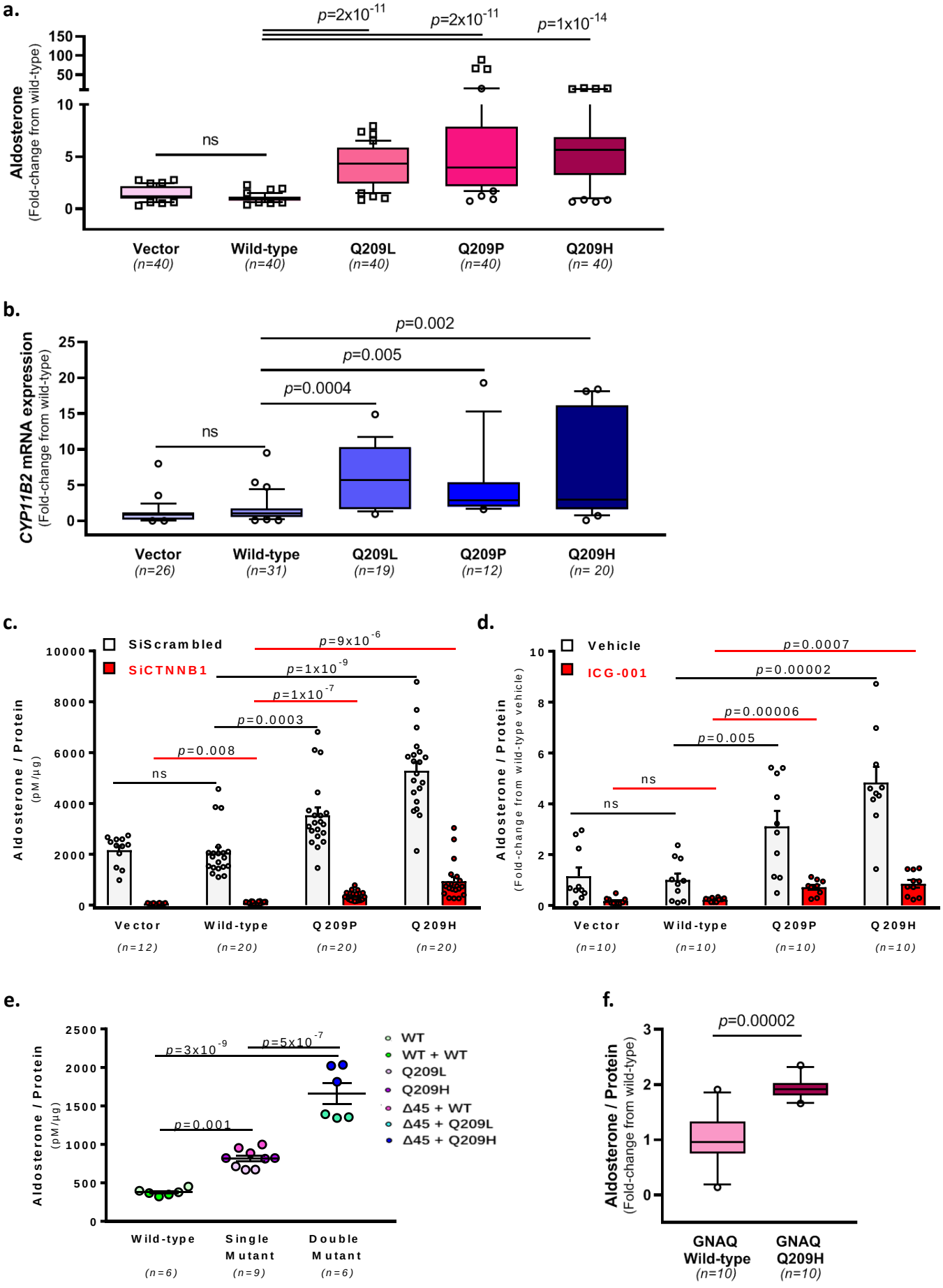

Figure 3 (a-g)

High LHCGR expression in *GNA11/Q* and *CTNNB1* double mutant aldosterone-producing adenomas (APAs) and double mutant co-transfected primary human adrenal cells.

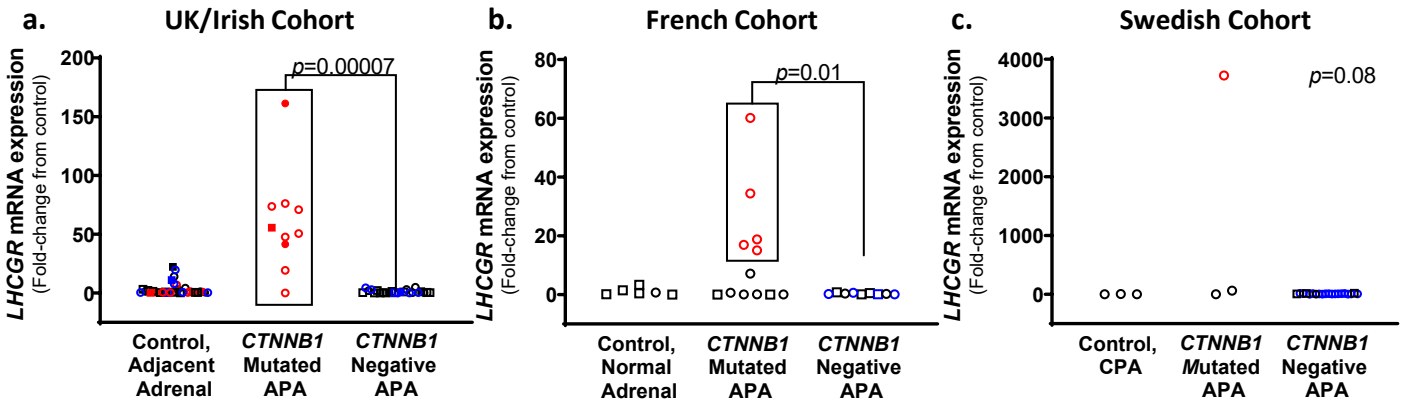

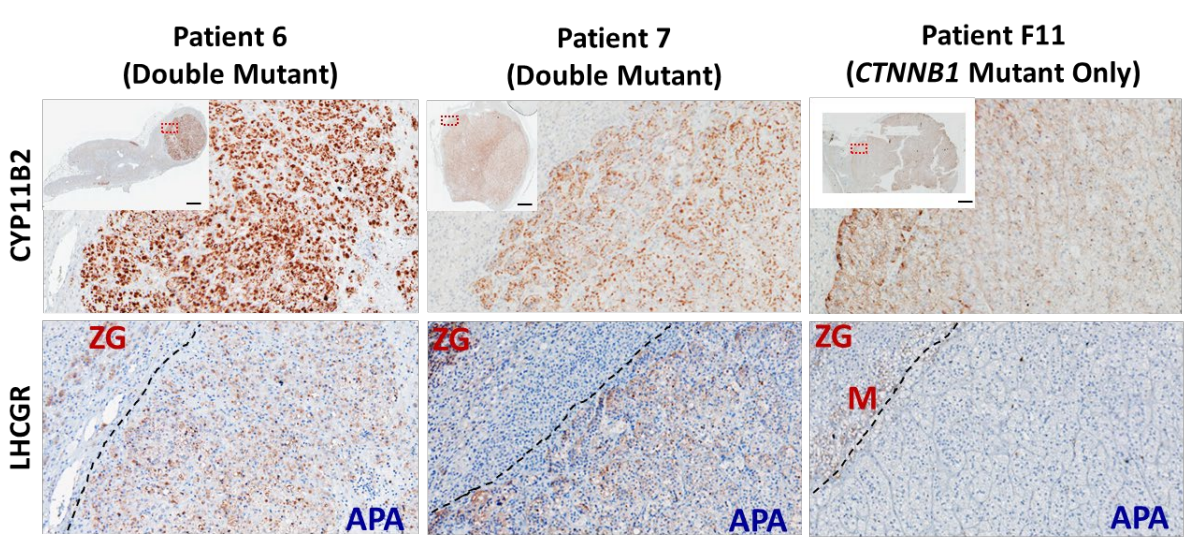

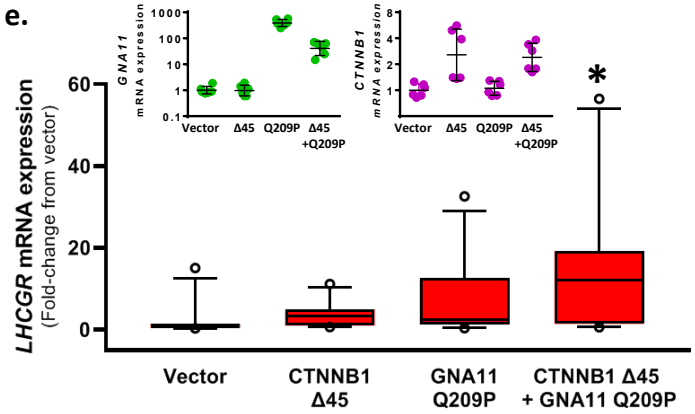

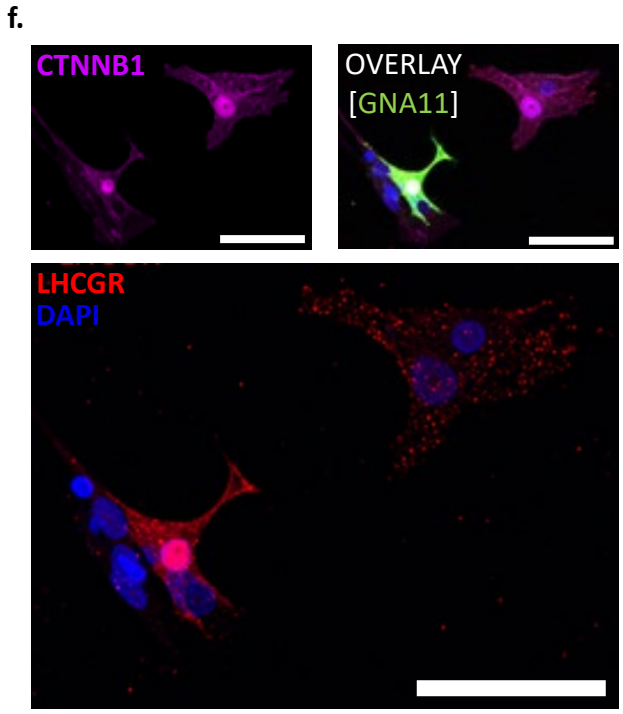

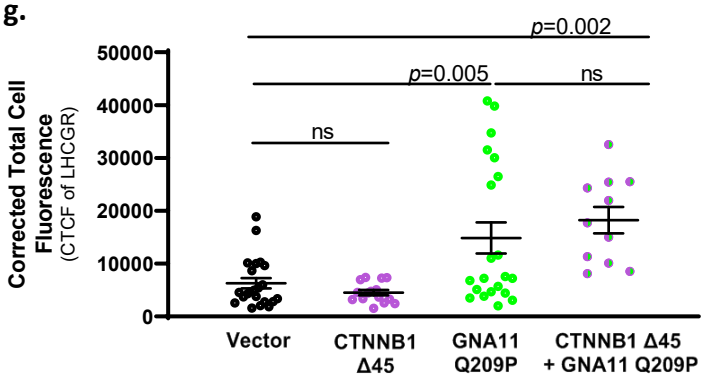

Figure 4 (a-f)

Gene expression profiles in *GNA11/Q* and *CTNNB1* double mutant adrenal cells.

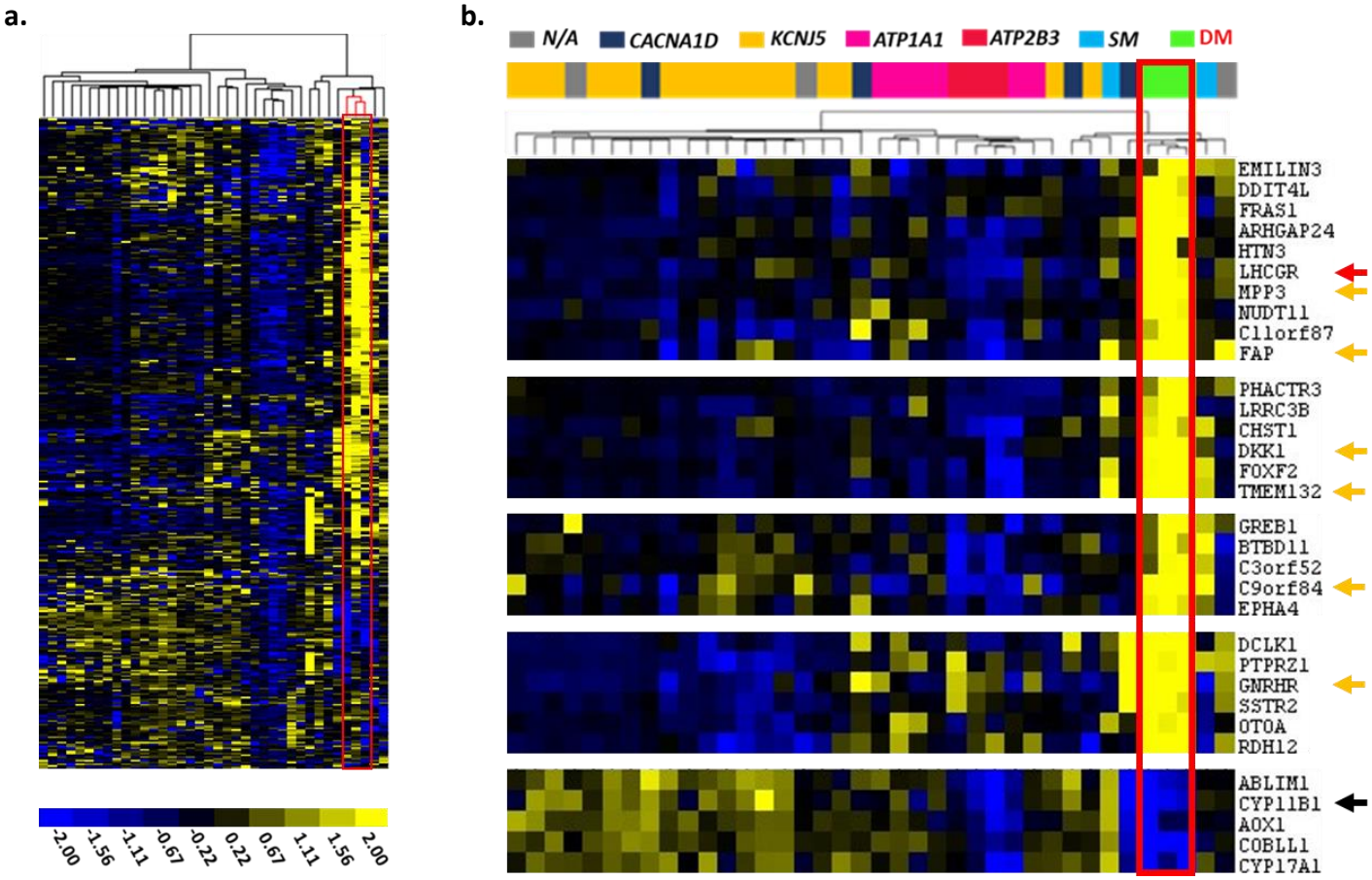

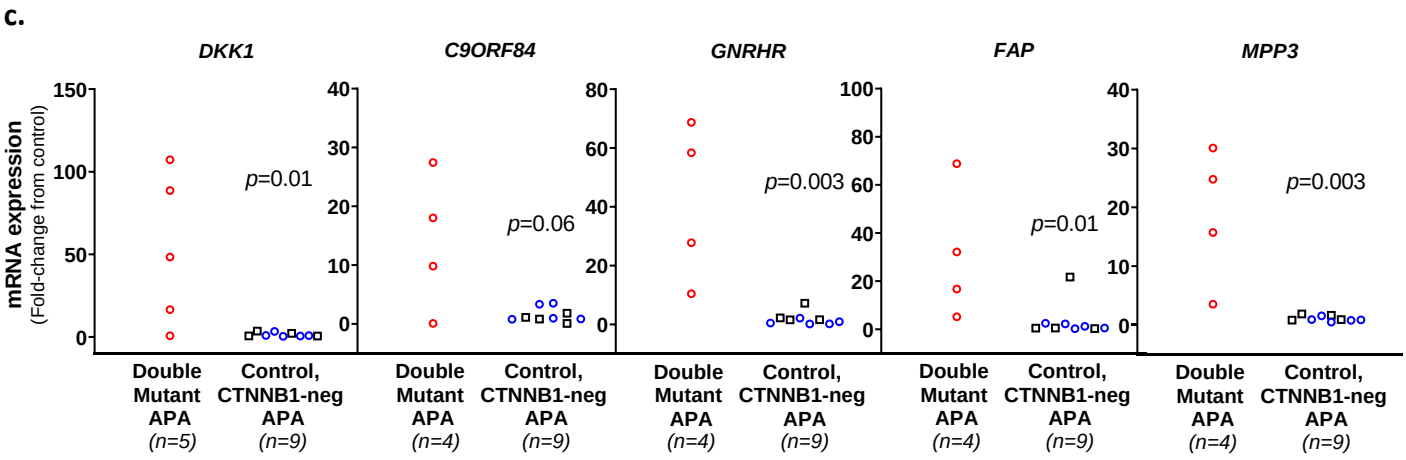

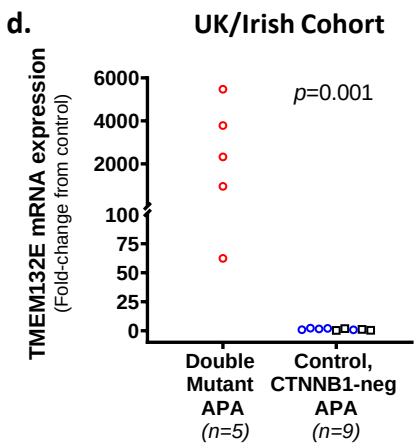

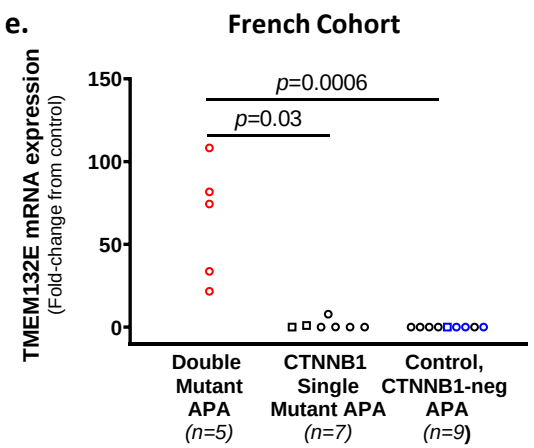

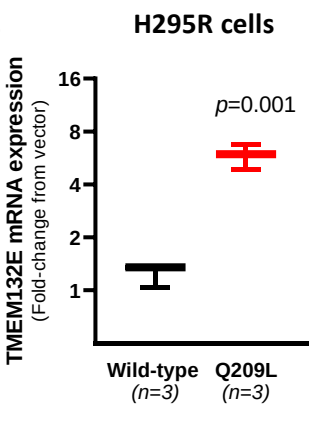

Figure 5 (a-b)

Aldosterone synthase (CYP11B2) and 11β-hydroxylase (CYP11B1) expression in *GNA11/Q and CTNNB1* double mutant APAs.

a.

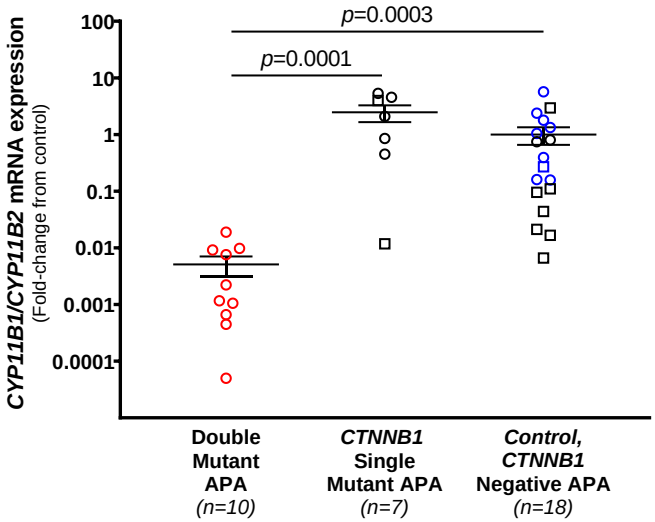

b.

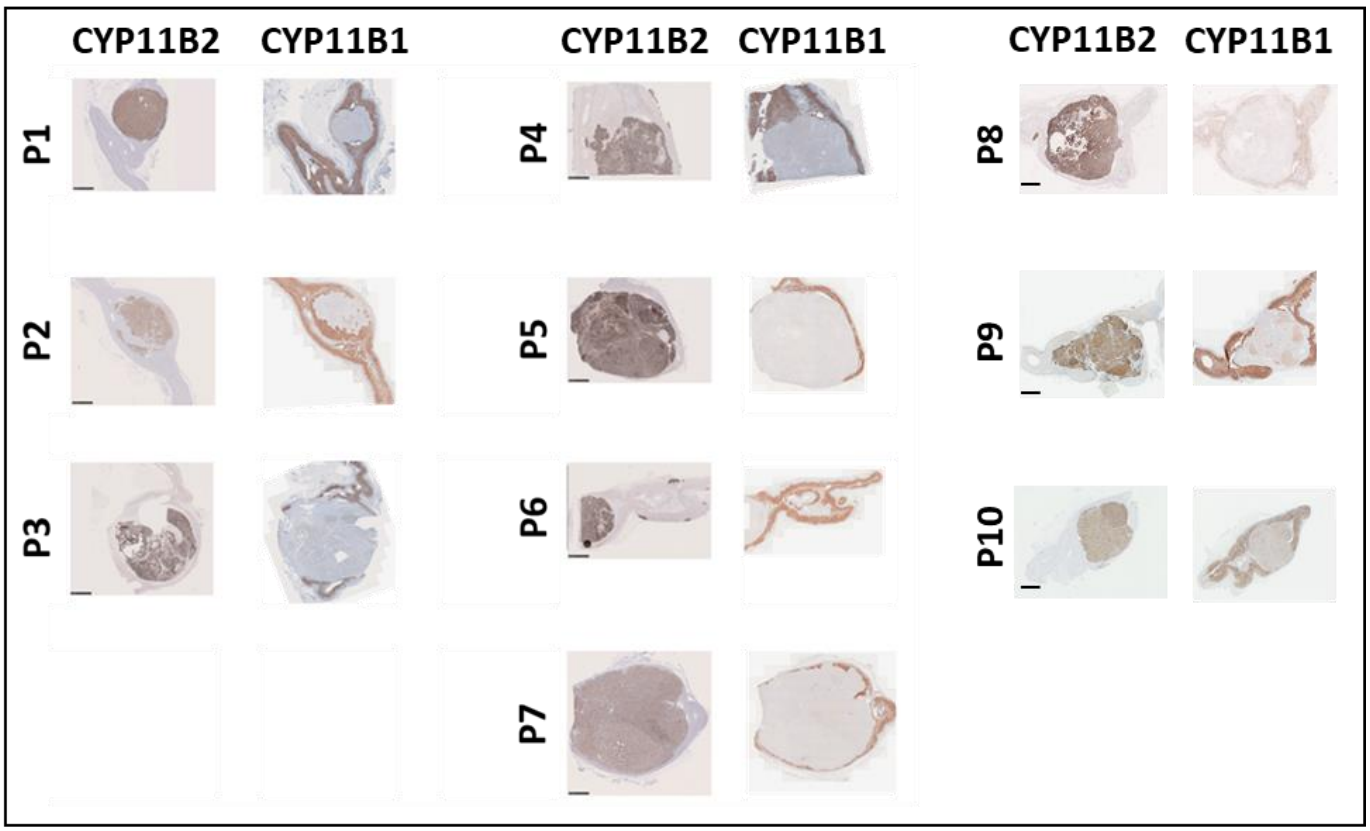

Figure 6 (a-f)

***GNA11* somatic mutations were found in the adjacent adrenals to double mutant APAs of Patient 7 (a-c) and Patient 1 (d-f).**

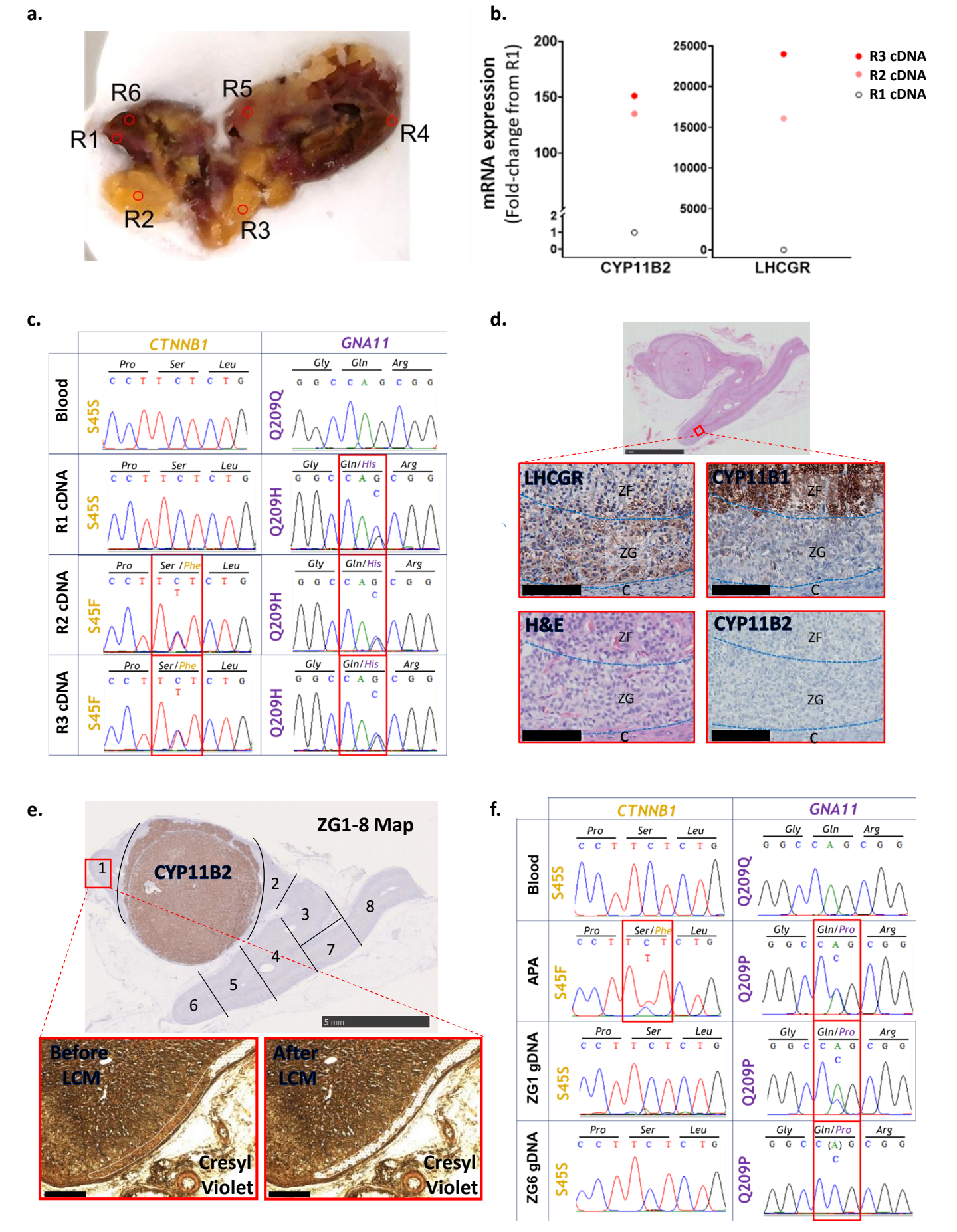

Extended Data Figure 1 (a-b)

APA 351T cells transfected with *CTNNB1* (untagged plasmid) and *GNA11* (GFP tagged plasmid) wild-type or Q209P.

a.

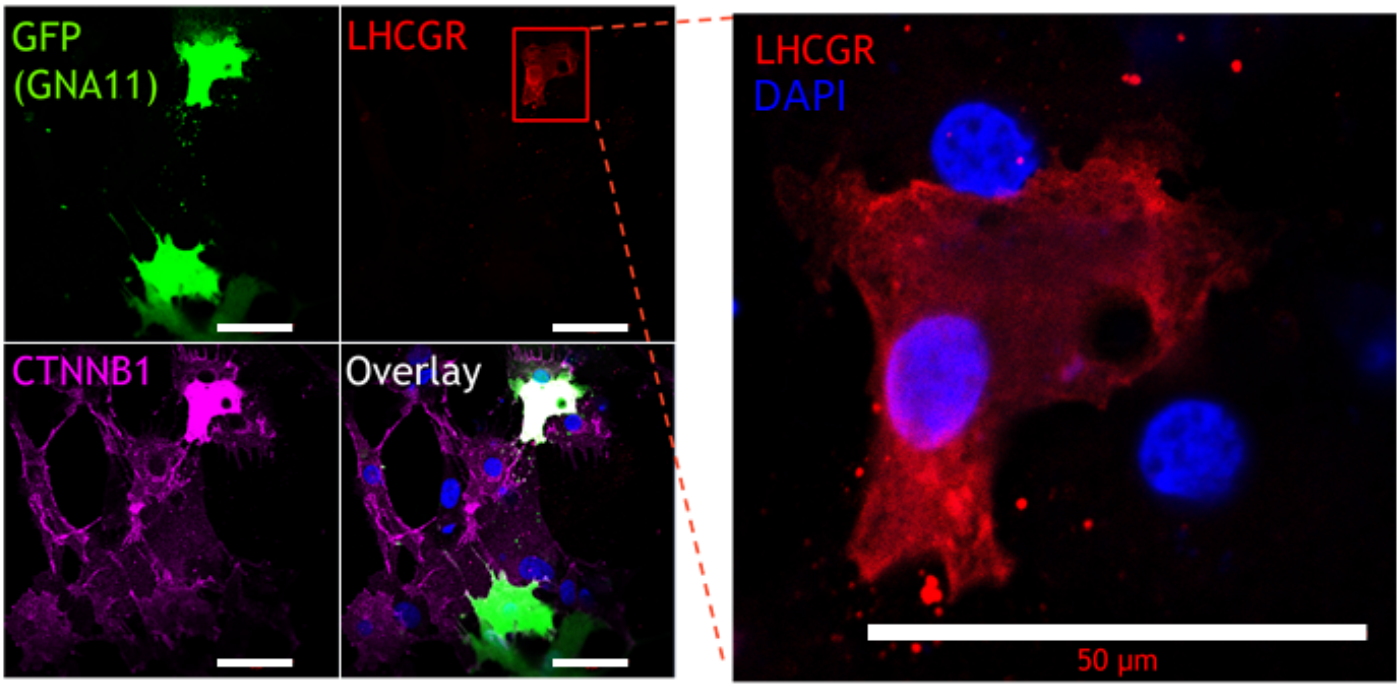

b.

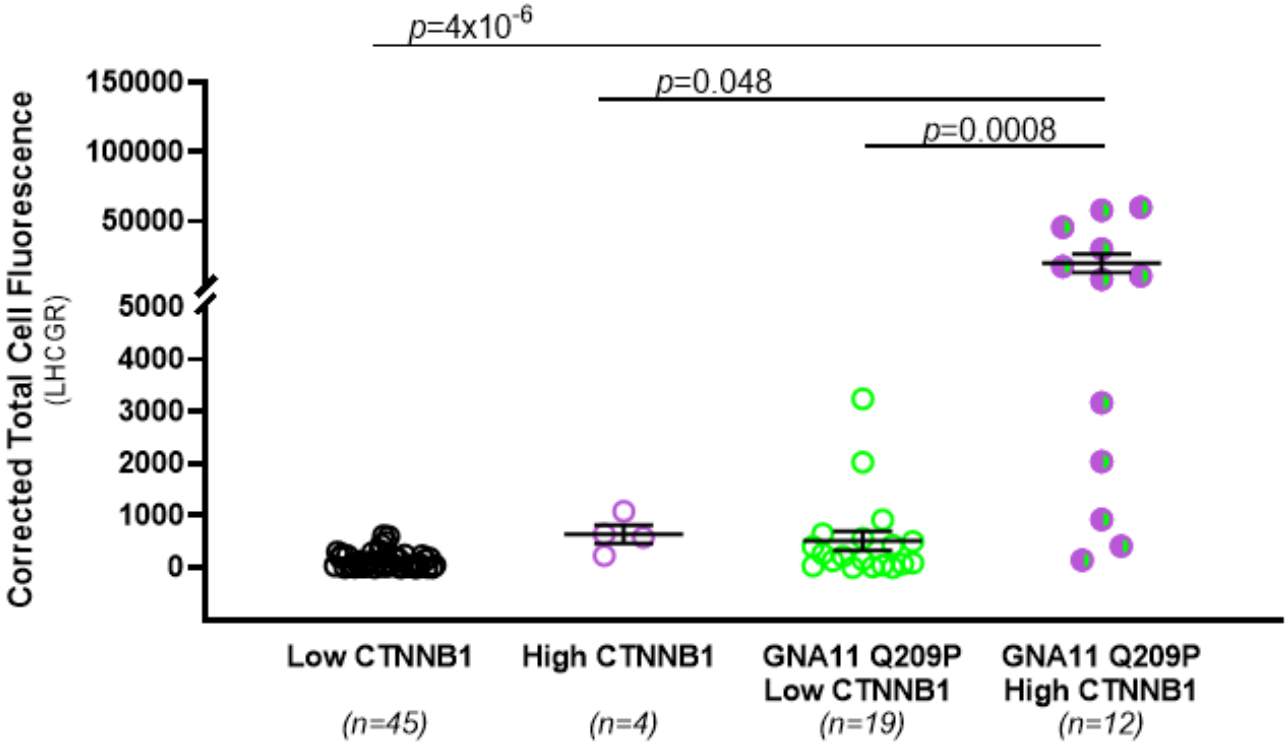

Extended Data Figure 2 (a-d)

***GNA11* somatic mutations were found in the adjacent adrenal to double mutant APA of Patient 6.**